nature neuroscience

Article

https://doi.org/10.1038/s41593-023-01483-5

Neural patterns differentiate traumatic from sad autobiographical memories in PTSD

Received: 29 July 2022

Accepted: 5 October 2023

Published online: 30 November 2023

Check for updates

Ofer Perl[1,2,3], Or Duek[4,5,6], Kaustubh R. Kulkarni[1,2,3], Charles Gordon[5,6], John H. Krystal[5,6], Ifat Levy[7,8], Ilan Harpaz-Rotem[5,6,8,9] ✉ & Daniela Schiller[1,3,9] ✉

For people with post-traumatic stress disorder (PTSD), recall of traumatic memories often displays as intrusions that differ profoundly from processing of 'regular' negative memories. These mnemonic features fueled theories speculating a unique cognitive state linked with traumatic memories. Yet, to date, little empirical evidence supports this view. Here we examined neural activity of patients with PTSD who were listening to narratives depicting their own memories. An intersubject representational similarity analysis of cross-subject semantic content and neural patterns revealed a differentiation in hippocampal representation by narrative type: semantically similar, sad autobiographical memories elicited similar neural representations across participants. By contrast, within the same individuals, semantically similar trauma memories were not represented similarly. Furthermore, we were able to decode memory type from hippocampal multivoxel patterns. Finally, individual symptom severity modulated semantic representation of the traumatic narratives in the posterior cingulate cortex. Taken together, these findings suggest that traumatic memories are an alternative cognitive entity that deviates from memory per se.

Personal memory is at the core of post-traumatic stress disorder (PTSD)[1]. Research on the neural mechanism of PTSD has largely focused on nonpersonal basic learning and memory paradigms[2]. It is still unclear how traumatic memories differ from negative nontraumatic autobiographical memories. Is a traumatic memory an exceptionally strong manifestation of autobiographical memory or a different neural representation altogether?

To examine this, we needed to factor in differences across individual traumatic narratives and the idiosyncratic experiences that they evoked, and extract from them the common markers operating in a trauma-driven state. With this in mind, we designed a study that examines the neural responses of patients with PTSD to their own personal traumatic memory in the form of a structured, fully annotated, audio narrative. We compared traumatic memory, within each participant, to a negatively valenced, nontraumatic, sad memory and a calm positive memory.

Previous research has established the role of the hippocampus in the construction of relational cognitive maps, on to which events are bound across space and time to form episodic memories[3–5]. It is through this tracking of sequences of events that the hippocampus is necessary

[1]Center for Computational Psychiatry, Icahn School of Medicine at Mount Sinai, New York, NY, USA. [2]Department of Psychiatry, Icahn School of Medicine at Mount Sinai, New York, NY, USA. [3]Nash Family Department of Neuroscience, Icahn School of Medicine at Mount Sinai, New York, NY, USA. [4]Department of Epidemiology, Biostatistics and Community Health Sciences, School of Public Health, Ben-Gurion University of the Negev, Beer-Sheva, Israel. [5]Department of Psychiatry, Yale University School of Medicine, New Haven, CT, USA. [6]The National Center for PTSD, VA CT Healthcare System, West Haven, CT, USA. [7]Departments of Comparative Medicine and Neuroscience, Yale University, New Haven, CT, USA. [8]Department of Psychology and the Wu Tsai Institute, Yale University, New Haven, CT, USA. [9]These authors contributed equally: Ilan Harpaz-Rotem, Daniela Schiller.
✉e-mail: ilan.harpaz-rotem@yale.edu; daniela.schiller@mssm.edu

for the construction of a narrative from discrete events[6,7]. In turn, the hippocampus also governs the ensuing retrieval of such events[8,9]. The hippocampus is in fact so central to the maintenance of episodic memory that creating lesions in it results in grave deficits in mnemonic abilities, to the point of global anterograde amnesia in humans[10].

Impairments to hippocampal processes are focal to PTSD pathophysiology[11]. Evidence suggests that PTSD is associated with structural abnormalities (predominantly a reduction in volume), as well as reduced functional connectivity between the hippocampus and other regions of the default mode network (DMN) during rest[12,13]. In the context of encoding the traumatic memory itself, aberrations in hippocampal function are thought to contribute to the paradoxical mnemonic sequelae commonly observed in PTSD—difficulty in voluntary coherent recall alongside detailed involuntary intrusions of the traumatic memory[14,15]. All in all, our understanding of the impact of PTSD on the spectrum of hippocampus-mediated mnemonic processes is still murky[16].

Emotional memories—episodic memories that elicit emotions at retrieval—often engage the amygdala[17]. Functionally, the amygdala is considered to be one component in a broader neurocircuitry model implicated in PTSD, comprising the hippocampus and medial prefrontal cortex[18]. Generally, the amygdala shows hyperresponsivity to both nonspecific, threat-related stimuli[19] and personal trauma reminders in PTSD[20–22]. Amygdala activation during memory encoding modulates the memory's explicit subsequent strength[23], evaluated through its persistence, accuracy and vividness[24]. Whether the amygdala itself serves as an 'auxiliary' site to support the storage of emotional memory is still being debated[25–27].

In the present study, we examined whether and how the brain differentiates between traumatic and sad autobiographical memories. We hypothesized that, across patients with PTSD, semantic similarity would correspond to neural similarity: if the personal memories of two participants were semantically close, their patterns of neural responses while listening to the audio recording of these memories should be similar as well. If traumatic and sad memories were just different cases of autobiographical memories, we should observe semantic-to-neural correspondence across pairs of traumatic memories and pairs of sad memories alike.

However, if traumatic autobiographical memories depart from—rather than being a version of—sad autobiographical memories, then we would observe the semantic-to-neural relationship only for sad, but not traumatic, memories. Our hypothesis further suggests that a shared neural representation will allude to a shared underlying neural mechanism. If the effect does not extend to pairs of traumatic memories across participants, despite their semantic similarity, this may imply that traumatic memories deviate from the neurotypical mechanisms of other sad, nontraumatic, autobiographical memories.

If traumatic memories differ from 'normal' sad memories in their hippocampal representation, what might be their alternative representation? Based on qualitative depictions, traumatic memories are not experienced as memories as such, but more as a present experience. They are felt in the moment rather than as a remote event in the past[28–30]. Traumatic memories are also more difficult to construe as a coherent narrative[31,32]. Indeed, a great deal of psychotherapy is geared toward reconstructing the traumatic event as a narrative that is embedded within life-long memories, attempting to distance the past trauma from the current safe present[15]. Such felt internal re-experiencing, which is momentarily disconnected from the external world and is not strictly embedded in time and space, may be supported by the DMN, particularly its central hub, the posterior cingulate cortex (PCC)[33–35]. The PCC has been demonstrated to be heavily implicated in both narrative comprehension and autobiographical memory processing[33,36], and particularly in emotional memory imagery[37]. Alterations in PCC function and connectivity are specifically focal in PTSD[38–40].

Considering this evidence, we hypothesized that, if a mechanistic difference between traumatic and sad memories exists, it would be detected in hippocampal and PCC neural patterns. If traumatic memories diverge from normal memory representation, we expect semantic-to-neural mapping in the hippocampus to emerge only for sad but not for traumatic memory. For traumatic memory, we set out to ask whether the relationship between semantic and neural representation will emerge in the PCC, given the evidence supporting both its roles in autobiographical memory processing and narrative comprehension and, conversely, evidence for dysfunction in PTSD. As a control comparison, we did not expect such differentiation, or any pattern representation related to the semantic content of memories in the amygdala, given the role of this region primarily in signifying emotional saliency rather than semantic content.

To test these hypotheses, we examined the neural activity of patients with PTSD who were listening to narratives depicting their own memories: traumatic, sad and calm. We used an intersubject representational similarity analysis (IS-RSA) of semantic content and neural patterns across participants to reveal a differentiation in neural representation by narrative type. Such differentiation will indicate that traumatic event representation is a cognitive state that deviates from memory as such.

Results

Twenty-eight participants (age = 38.2 ± 10.4 years, 11 females) diagnosed with PTSD (Clinician-Adminstered PTSD Scale (CAPS) score = 41.2 ± 8.3) underwent reactivation of autobiographical memory through script-driven imagery while undergoing functional magnetic resonance imaging (fMRI). First, to generate stimuli that are based on participants' autobiographical memory, we used an imagery development procedure. Participants elaborated on three types of autobiographical memories: (1) the 'PTSD' condition: the traumatic event associated with their PTSD (*Diagnostic and Statistical Manual of Mental Disorders*, 5th edition (DSM-5) (ref. 1), Criterion A; common examples were combat, sexual assault and domestic violence); (2) the 'Sad' condition: a sad meaningful, but nontraumatizing experience (common examples were death of a family member or pet)'; and (3) the 'Calm' condition: a positive, calm event (common examples were memorable outdoor activities). These highly personal and variable depictions of autobiographical memory were then systematically arranged into an approximately 120-s audio clip (referred to henceforward as 'script' or 'narrative', interchangeably), narrated by a member of the research staff. All scripts were composed with ample attention to a common rigid structure, into which the individual autobiographical memory was incorporated. Notably, 'PTSD' and 'Sad' narratives were scripted to maximize their structural similarity to control for content and arousal (Methods). Participants listened to this new rendition of their autobiographical memory for the first time while undergoing fMRI (Fig. 1a).

We provided word-cloud plots depicting word occurrence per each individual script (Supplementary Fig. 1) as well as bigram word-cloud plots clustering phrases common to each script type ('Calm', 'Sad', 'PTSD') (Supplementary Fig. 2).

Basic group inference in cognitive neuroscience, and neuroimaging, in particular, relies on the detection of shared stimulus-induced signals of greater amplitude than the noise or idiosyncratic signals in these systems[36]. Autobiographical memories are rarely generated in a controllable lab setting and therefore differ in their content. However, at the same time, autobiographical memory recall may elicit common cognitive states (for example, mental time travel) that are potentially subserved by common neural substrates across individuals. In the present study, the sensory stimuli used for reactivation were based on idiosyncratic experiences to invoke a common cognitive state—the reactivation of traumatic autobiographical memories. During recruitment, participants were not screened for a specific trauma type. This enabled us to span a wide range of themes, some of which were present in 'PTSD' and 'Sad' conditions. For example, a narrative describing the death of a loved one can meet the PTSD Criterion A classification for one

https://doi.org/10.1038/s41593-023-01483-5

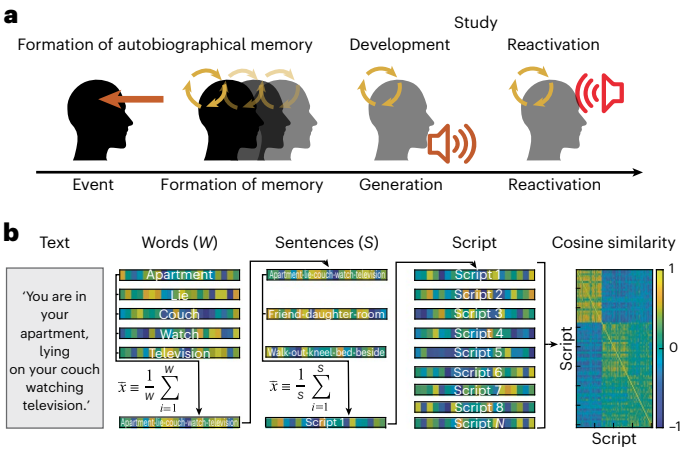

Fig. 1 | Experimental paradigm and semantic analysis framework. **a**, Experimental paradigm for script-based autobiographical memory reactivation. At some point before enrollment, an event was perceived and an autobiographical memory formed. Since then, this memory will have undergone an unknown number of recalls and reconsolidation iterations. During the study, participants once again recalled this memory, this time while verbalizing it as part of the imagery development procedure. These recollections were incorporated into a new narrative-form rendition of the autobiographical memory, which was played to the participants for the first time while undergoing functional imaging, to reactivate this autobiographical memory once again. **b**, Semantic similarity of autobiographical narratives using word embedding. Each indexable word in the script was assigned a 300-dimensional vector representation (for example, 'apartment', 'lie'). Sentence vectors were represented as the average of word vectors comprising them (for example, tokenized, such as 'apartment lay couch watch television') and scripts represented as the average of the sentences in them. Pairwise semantic similarity across participants was calculated using cosine similarity.

participant and thus be associated with a traumatic autobiographical narrative, yet be regarded as a 'Sad' autobiographical memory (that is, nontraumatizing) for another. Therefore, assigning a continuous, parametric relationship to similarity between autobiographical memories may allow comparison of neural representation of relatable autobiographical memories in light of their clinical outcomes, and critically—to compare the representation of relatable autobiographical memories in light of their clinical outcomes—'PTSD' or nontraumatizing.

Semantic analysis of similarity in autobiographical memory

To quantify similarity between autobiographical memory-based narratives across individuals and conditions, we applied a word-embedding approach—a computational linguistic tool used to quantify distances between text-based semantics[41]. In brief, words are presampled from gigantic text corpora and are then embedded in a high-dimensionality space according to local co-occurrences. The derived semantic space allows one to infer relational structure between concepts according to their distance. Such tools were previously used to uncover neural representations of semantic spaces[42] with both functional imaging[43] and invasive recordings[44].

We used MATLAB's word2vec with a pretrained embedded space for one million words in the English language[45]. Each word was assigned a 300-dimensional vector representation. In our analytical hierarchy, sentence vectors were represented as the average of the word vectors comprising them. Similarly, scripts were represented as the average representation of their sentences (Fig. 1b). The high dimensionality of the semantic dataset is difficult to interpret visually. We, therefore, applied *t*-distributed stochastic neighbor embedding (*t*-SNE), a method for dimensionality reduction, to the data to cluster narratives based on the semantic similarity of their content, and projected this dimensionality-reduced dataset on to a three-dimensional (3D) space.

We observed that both types of negatively valenced narratives—'PTSD' and 'Sad'—formed overlapping clusters in semantic space, whereas 'Calm' narratives were grouped in a separate part of the space (Fig. 2a). Additional 2D projections of the semantic space are available in Supplementary Fig. 3. This qualitative visualization affirmed that the semantic content of 'PTSD' and 'Sad' autobiographical memories is comparable and thus 'Sad' scripts are poised to provide a valid control for the 'PTSD' scripts.

We next measured semantic similarity using cosine similarity between the 300-dimension vectors representing the scripts. The resulting semantic similarity matrix comprised the three script types ('PTSD', 'Sad' and 'Calm') of 28 participants yielding a 84 × 84 matrix in total. Script types were grouped to aid in visualization of 'type' clusters off the diagonal (Fig. 2b).

We applied a second, complementary method of semantic contextual embedding to the scripts. This transformer model—BERT, implemented in MATLAB—was able to provide representations that were shaped by intrasentence dynamics (Supplementary Fig. 4a,b). Both the resulting semantic similarity matrices were highly correlated (Pearson's correlation, $r = 0.88$, $P < 0.00001$, $n = 3{,}486$; Supplementary Fig. 4c), suggesting that both models were able to capture similar semantic concepts.

In addition to dimensionality reduction, we calculated cross-category similarity and observed that the 'PTSD' and 'Sad' narratives showed a higher cross-category semantic similarity than other cross-category comparisons (similarity (*r*): 'PTSD':'Sad' = 0.059 ± 0.159; 'Calm':'Sad' = −0.274 ± 0.147; 'Calm':'PTSD' = −0.224 ± 0.150; analysis of variance (ANOVA): $F(2, 2{,}351) = 1{,}094.75$, $P < 1 \times 10^{-300}$; $\eta_p^2 = 0.325$) (Fig. 2c). This semantic resemblance can be attributed to the themes shared by both negatively valenced scripts and the systematically controlled structure and shared phrases that were used.

In a complementary analysis, we quantified pairwise similarity within each of the three script categories. As expected, we observed that within-category scripts displayed high semantic similarity (similarity (*r*): 'PTSD' = 0.164 ± 0.139; 'Sad' = 0.237 ± 0.174; 'Calm' = 0.413 ± 0.174; one-sample Student's *t*-test versus 0: all $P < 1 \times 10^{-300}$). Furthermore, an ANOVA conducted on script types revealed a main effect of 'script' (ANOVA: $F(2, 1{,}133) = 231.80$, $P = 4.29 \times 10^{-85}$, $\eta_p^2 = 0.225$). Post hoc Student's *t*-tests further demonstrated that 'Calm' scripts had higher within-category similarity than 'Sad' scripts, and 'Sad' scripts had higher with-category similarity than 'PTSD' scripts (both $P < 0.0001$, Bonferroni corrected).

These results suggest that sad and traumatic memories in the cohort overlapped in themes and semantic content. This analysis laid foundations for asking whether the neural patterns associated with these memories will differ by their clinical classification: traumatic or sad. Thus, any ensuing neural differences between 'PTSD' and 'Sad' reactivations may present themselves on top of a maximally identical pool of stimuli. We note that, given their autobiographical nature and the use of a naturalistic paradigm, such stimuli may never be identical. However, establishing a 'handle' on the differences and commonalities of the narratives enables us to leverage those differences in a quantifiable manner to provide neural insight.

Validation of comparable psycholinguistics between scripts

We applied a series of validations to script content using external psycholinguistic rating databases (see Methods for details). We focused on concreteness, imageability and valence, given that these factors may act as possible confounders in a subsequent neural investigation based on imagery and memory reactivation (Supplementary Fig. 5). Repeated measures ANOVA (rmANOVA) indicated significant differences across the three conditions (PTSD, sad and calm) for the three variables (concreteness: rmANOVA $F(2, 54) = 14.02$, $P = 1.24 \times 10^{-5}$; valence: rmANOVA $F(2, 54) = 6.03$, $P = 0.004$; imageability: rmANOVA $F(2, 54) = 12.37$, $P = 3.77 \times 10^{-5}$).

https://doi.org/10.1038/s41593-023-01483-5

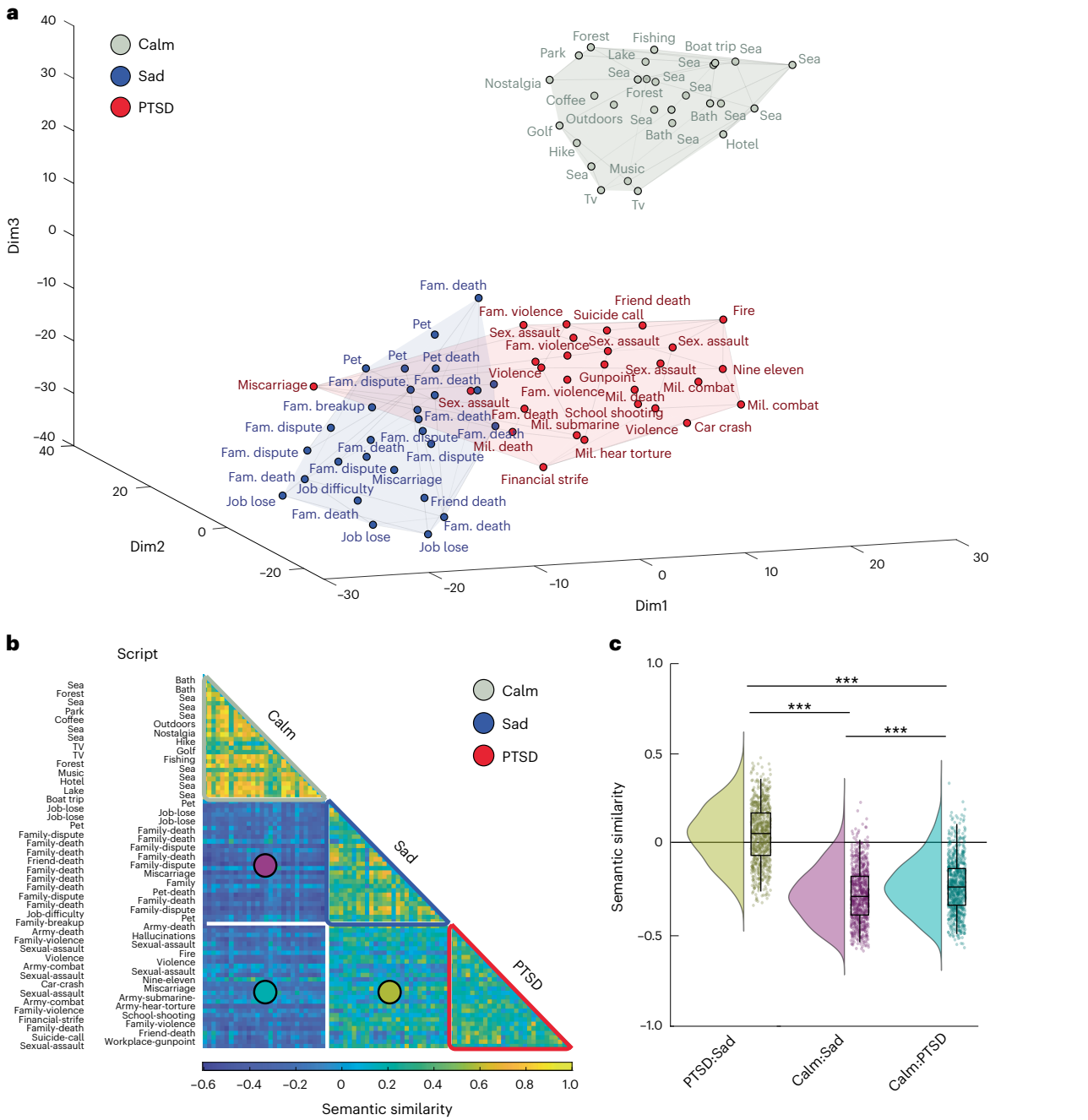

Fig. 2 | Semantic similarity across script types. a, Clustering of semantic similarity across script types using *t*-SNE. For the *t*-SNE embedding of scripts, each dot represents a single script, projected on to a 3D space. Colored volumes are continuous areas in space occupied by each script type. Color denotes script type ('PTSD', red; 'Sad', blue; 'Calm', gray). Note the overlap of the 'PTSD' and 'Sad' semantic content. The text adjacent to datapoints is a general title of narrative content, generated by the researchers. Fam., family; Mil., military; Sex., sexual. Some titles were omitted to prevent clutter. **b**, Pairwise similarity of semantic content of scripted narratives. Semantic pairwise cosine similarity was presented for all scripted narratives. Within-category similarity is marked in colored triangles off the matrix diagonal ('PTSD', red; 'Sad', blue; 'Calm', gray). Cross-category similarity is marked in colored circles in distinct square sectors of the matrix ('PTSD:Sad', yellow; 'Calm:Sad', magenta; 'Calm:PTSD', teal). Text labels next to matrix rows are general titles of narrative content, generated by the researchers. **c**, Semantic similarity across script types. Raincloud plots illustrate the distribution of pairwise semantic similarity between pairs of script types. Next to each raincloud is a box plot portraying the same data ($n = 784$). Median-centered boxes show 25th and 75th quantiles and whiskers extend to 2nd and 98th quantiles (ANOVA: $F(2, 2{,}351) = 1{,}094.75$, $P < 1 \times 10^{-300}$; $\eta_p^2 = 0.325$, post hoc, two-sided, two-sample Student's *t*-tests (Tukey's correction): 'PTSD:Sad': $t = -7.43$, $P < 0.001$; 'Calm:Sad': $t = -43.15$, $P < 0.001$; 'Calm:PTSD': $t = -35.71$, $P < 0.001$). $^{***}P < 0.001$.

Post hoc paired Student's *t*-tests and Bayesian analyses confirmed no differences between 'PTSD' and 'Sad' scripts in concreteness ($t(27) = -1.69$, $P = 0.207$ (Bonferroni corrected); base factor $(BF)_{10} = 0.706$) or valence ($t(27) = 1.36$, $P = 0.707$ (Bonferroni corrected); $BF_{10} = 0.461$). We observed a difference in imageability ratings between 'PTSD' and 'Sad' scripts such that 'PTSD' scripts had a higher imageability score ($t(27) = 4.87$, $P = 3.8 \times 10^{-5}$ (Bonferroni corrected); $BF_{10} = 565$). These results confirm that psycholinguistic features in general cannot explain the differences observed in the semantic-to-neural relationship between conditions. Specifically, lower imageability cannot

https://doi.org/10.1038/s41593-023-01483-5

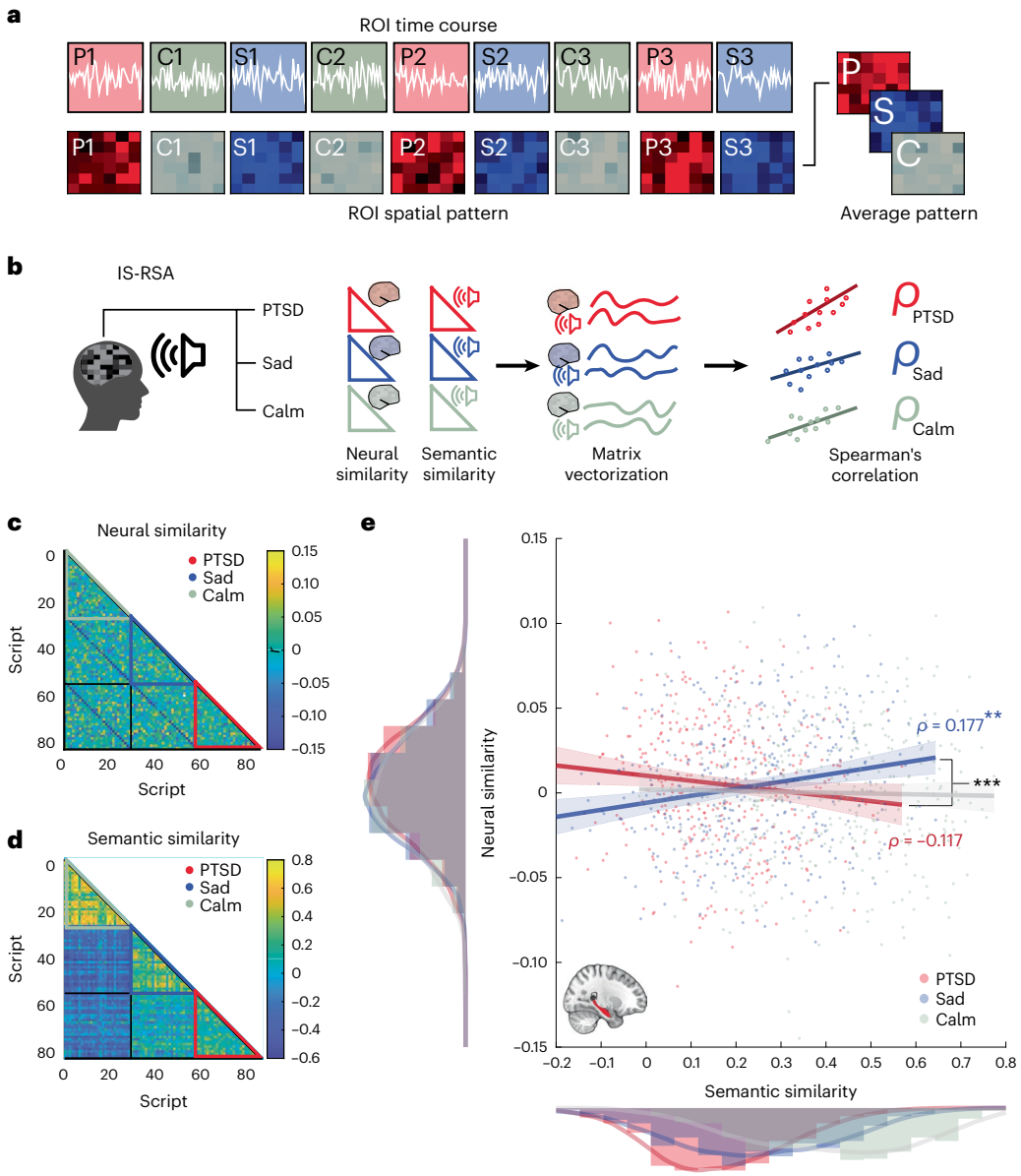

Fig. 3 | Semantic-to-neural similarity analysis of hippocampal patterns. **a**, Extraction of spatial patterns. Each script narrative ('PTSD', 'Sad', 'Calm') was played three times in the scanner. Spatial patterns were extracted from the ROIs and averaged across repeated presentations to generate an average pattern associated with each script reactivation. **b**, IS-RSA. We carried out three independent IS-RSAs in which intersubject variability during script reactivation was captured using two subject-by-subject matrices: one depicting neural pattern pairwise similarity and the other depicting semantic pairwise similarity. Spearman's rank correlation was calculated for each pair of vectorized similarity matrices to provide a correlation coefficient tying semantic and neural representations of 'PTSD', 'Sad' or 'Calm' narratives. **c**, Hippocampus: neural similarity matrix. Script-by-script neural cosine similarity matrix for spatial patterns extracted from the hippocampus during script reactivation. Within-category similarity is marked in colored triangles off the matrix diagonal ('PTSD', red; 'Sad', blue; 'Calm', gray). **d**, Semantic similarity matrix. Script-by-script semantic similarity of scripted narratives. Within-category similarity is marked in colored triangles off the matrix diagonal ('PTSD', red; 'Sad', blue; 'Calm', gray). **e**, Hippocampus: semantic-to-neural IS-RSA. IS-RSA was conducted on pairwise similarity of semantic content and neural patterns in the hippocampus. Each datapoint is one pairwise comparison ($n = 378$ per condition). Analysis was iterated per script type ('PTSD', red; 'Sad', blue; 'Calm', gray). Histograms along axes depict similarity distribution, a thick trace depicts estimated density and colors correspond to the main legend. Regression lines are an approximate visualization of Spearman's correlation, ρ, coefficients for IS-RSA in 'PTSD' (red, $\rho = -0.117$, $P_{(\text{FDR corrected})} = 0.104$) and 'Sad' scripts (blue, $\rho = 0.177$, $P_{(\text{FDR corrected})} = 0.005$). In the two-sided tests, the error bands indicate 95% confidence intervals (CIs). $^{**}P < 0.05$; $^{***}P < 0.001$.

explain the lack of hippocampal involvement in PTSD—despite higher level imageability scores, the 'PTSD' scripts do not show increased neural similarity.

Intersubject representational similarity analysis

All participants listened to each script type three times during the functional scan. We used general linear modeling (GLM) to measure brain activity during script reactivation compared with baseline (Methods). Given our previous interest in the involvement of the hippocampus, amygdala and PCC in the processing of traumatic autobiographical memories in PTSD, we extracted signals from these structures using the Harvard–Oxford probabilistic atlas (hippocampus and amygdala) and a GLM-derived functional region of interest (ROI) in the PCC to conduct ROI-targeted analyses.

To enhance signal to noise for the detection of the common pattern elicited by the repeated stimuli across different presentations, the time courses were averaged across the three repeats of the script per ROI within the course of a single scan. The voxel time course of this average run was collapsed across time to generate a spatial pattern associated with the reactivation of each autobiographical memory. Finally, we generated a neural similarity matrix by calculating the pairwise Pearson's correlation coefficient between the spatial patterns of all scripts. The dimensions of this matrix were identical to the one storing the narratives' semantic similarity (28 participants × 3 script types) (Fig. 3a).

To account for the idiosyncratic nature of autobiographical memories, we used IS-RSA to relate the personalized semantic content of the scripts with neural representations acquired during script reactivation. Generally speaking, IS-RSA assesses how intersubject variability in neural patterns relates to individual differences in behavioral measures or traits and, in this case, autobiographical memories. The semantic–neural similarity coefficient indicates that the more the similar participants' semantic content, the more similar their neural patterns, while listening to their own autobiographical memories.

In IS-RSA, the neural and semantic similarity matrices were vectorized and correlated (Spearman's correlation) within each category of script type, yielding three correlation coefficients ('rho', ρ) per ROI, one for each script type (Fig. 3b). The first IS-RSA that we conducted related between-participant neural similarity of hippocampal patterns (Fig. 3c) with the between-participant semantic similarity matrix computed before (Fig. 3d).

In the hippocampus, the IS-RSA uncovered a differentiation in semantic representation: semantic similarity scaled positively with neural similarity for 'Sad' narratives ('Sad', $\rho = 0.177$, $P_{(\text{FDR corrected})} = 0.005$, where FDR is false discovery rate) but not for 'PTSD' narratives ('PTSD', $\rho = -0.117$, $P_{(\text{FDR corrected})} = 0.104$) (Fig. 3e). (We further verified the strength of the link between semantic and neural matrices in the 'Sad' condition using Mantel's test for matrices correlation[46,47] which suggested a strong effect, $P = 0.001$.) A detailed breakdown of the three overlaid conditions in the hippocampal IS-RSA figure is available in Supplementary Fig. 6.

We then tested whether the two correlation coefficients of IS-RSA conducted on 'PTSD' and 'Sad' scripts and associated hippocampal patterns differed substantially. The correlation coefficients underwent a *z*-score transformation and the absolute difference between them was assigned a *P* value (Methods). We observed that, indeed, hippocampal IS-RSA representations of semantic content significantly differed as a function of script type (coefficient comparison (two-tailed) 'PTSD' versus 'Sad', hippocampus: $P_{(\text{FDR corrected})} = 0.00045$).

No semantic-to-neural representation in the amygdala and PCC

To examine whether the lack of semantic representation of traumatic autobiographical memories was specific to the hippocampus, we repeated the same IS-RSA with neural patterns extracted from the amygdala and PCC (Supplementary Fig. 7). Signals from the amygdala did not demonstrate a significant link between semantic content and neural patterns for either 'Sad' ($\rho = 0.066$, $P_{(\text{FDR corrected})} = 0.404$) or 'PTSD' narratives (amygdala: $\rho = -0.057$, $P_{(\text{FDR corrected})} = 0.269$). In addition, univariate analyses of GLM-derived parameter estimates suggested comparable levels of activation across script types in the amygdala (rmANOVA $F(2, 54) = 0.96$, $P = 0.39$, Bayesian rmANOVA: null model: $BF_M = 3.75$; 'script' model: $BF_M/BF_{10} = 0.27$).

To verify that this null effect is not a result of averaging left and right amygdala signals, we conducted IS-RSA and univariate analysis of the left and right amygdala separately, and observed no differences between 'PTSD' and 'Sad' conditions (IS-RSA: left amygdala: 'PTSD', $\rho = -0.03$, $P = 0.56$; 'Sad', $\rho = 0.024$, $P = 0.643$; coefficient comparison (two-tailed) 'PTSD' versus 'Sad', $P = 0.46$); right amygdala: 'PTSD', $\rho = -0.064$, $P = 0.21$, 'Sad', $\rho = 0.078$, $P = 0.129$; coefficient comparison (two-tailed) 'PTSD' versus 'Sad', $P = 0.051$; parameter estimates: left amygdala ($F(2, 54) = 1.19$, $P = 0.31$; Bayesian rmANOVA: null model: $BF_M = 3.29$; 'script' model: $BF_M/BF_{10} = 0.304$); right amygdala ($F(2, 54) = 0.541$, $P = 0.585$; Bayesian rmANOVA: null model: $BF_M = 5.25$; 'script' model: $BF_M/BF_{10} = 0.19$).

To define the PCC functionally, we generated a contrast comparing neural activity during narrative playback (all three script types were included) with the intertrial interval baseline. This contrast therefore factored activations for both positively and negatively valenced scripts. Signals from the PCC did not demonstrate a significant link between semantic content and neural patterns for either 'Sad' ($\rho = 0.049$, $P_{(\text{FDR corrected})} = 0.495$) or 'PTSD' narratives ($\rho = 0.079$, $P_{(\text{FDR corrected})} = 0.374$). See below additional results pointing to PCC involvement as a function of PTSD symptom severity. The univariate approach uncovered a main effect of script (rmANOVA $F(2, 54) = 6.24$, $P = 0.003$, Bayesian rmANOVA: null model: $BF_M = 0.08$; 'script' model: $BF_M/BF_{10} = 12.2$) but no difference between 'PTSD' and 'Sad' was observed in a post hoc planned comparison ($P = 0.558$, $BF_{10} = 0.236$). Finally, additional exploratory analysis on two other DMN regions that were functionally active during the task (medial prefrontal cortex) and left angular gyrus (both defined functionally by contrast: all conditions > baseline) did not reveal any effects (Supplementary Fig. 8)

Control analyses

We verified that the difference in semantic-to-neural mapping is not due to differences in mean amplitude between the conditions. To this end we conducted a GLM on the functional imaging data in which regressors related to all event types were created. The GLM included three separate regressors denoting the full duration of the three types of scripts: 'PTSD', 'Sad' and 'Calm' (see Supplementary Fig. 9 for activation maps). We extracted univariate parameter coefficients from the hippocampus and compared them using an rmANOVA which uncovered no differences between script types (rmANOVA $F(2, 27) = 0.67$, $P = 0.528$, Bayesian rmANOVA: null model: $BF_M = 5.7$; 'script' model: $BF_M/BF_{10} = 0.177$). In addition, a whole-brain GLM contrasting positive- and negative-valence scripts (('PTSD' + 'Sad') > 'Calm') uncovered no significant differences in hippocampal signals (see Supplementary Table 1 for clusters of activation). No clusters were also observed for the opposite contrast (('PTSD' + 'Sad') < 'Calm').

To control for possible habituation over the course of script playback, we repeated this approach while modeling the early and late parts of the script separately (roughly 1 min each). Focusing on the early part, we again observed comparable parameter estimates across script types (rmANOVA $F(2, 27) = 1.59$, $P = 0.212$, Bayesian rmANOVA: null model: $BF_M = 2.8$; 'script' model: $BF_M/BF_{10} = 0.36$). Taken together, these results mitigate concerns about confounding effects of different arousal levels across conditions.

We also sought to rule out a possible confounding factor in narrative similarity which may have been driven by similarity in low-level acoustic properties of the auditory stimuli. To this end we generated an acoustic similarity matrix (Methods) and conducted an IS-RSA using the acoustic and neural similarity matrices. We did not observe any significant representation of acoustic features in the hippocampal patterns, in both 'PTSD' and 'Sad' conditions (Supplementary Fig. 10).

Finally, we applied a battery of control analyses to test whether the low correlation coefficient values in the semantic-to-neural IS-RSA conducted on the 'Calm' scripts was the result of insufficient variance in the semantic content of the full set of this type of autobiographical memories.

To do this, we comprehensively mapped the link between semantic and neural similarity across script types. We iteratively generated five-script subsets of the original cohort and conducted IS-RSA on all possible combinations separately per script type ($n = 98{,}280 \times 3$). Next, we sorted the subsets by their semantic cosine similarity and directly compared the values of IS-RSA correlation coefficients of the hundred highest- and lowest-ranking subsets. We observed that, in both 'Calm' and 'Sad' scripts, higher semantic similarity was significantly associated

https://doi.org/10.1038/s41593-023-01483-5

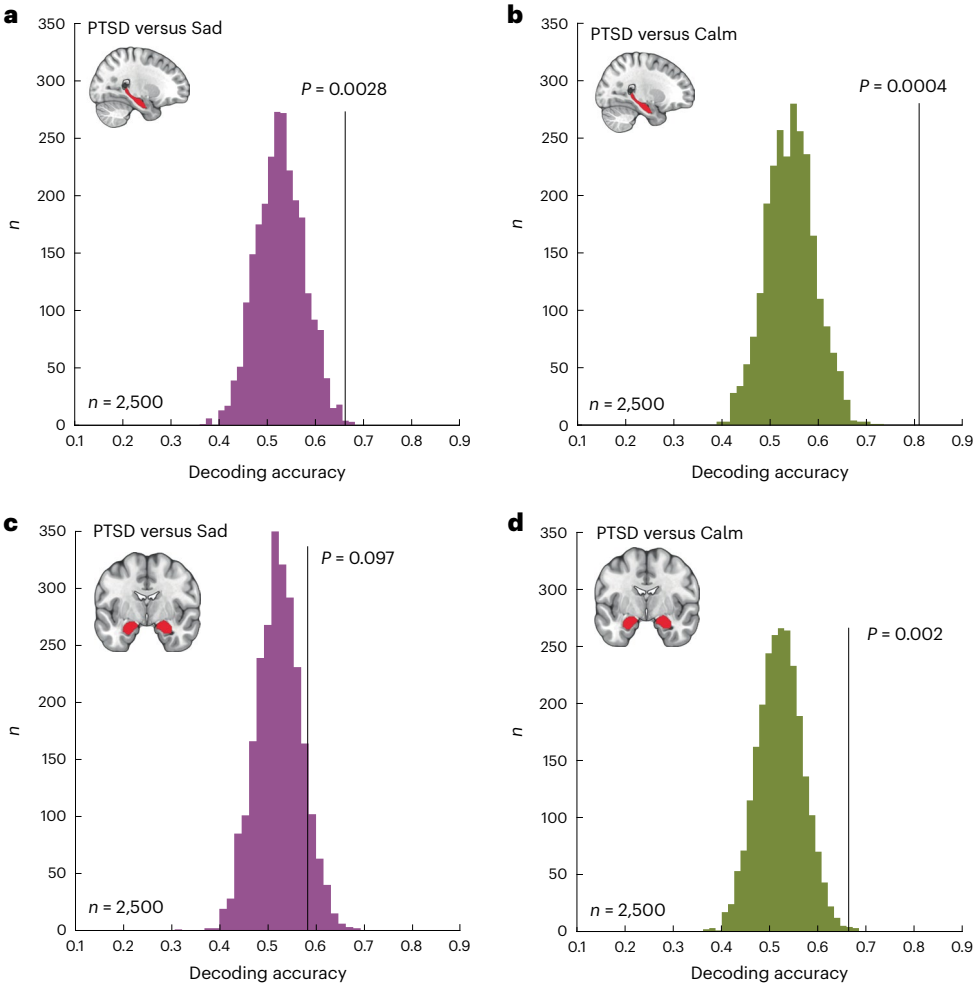

Fig. 4 | Memory type can be decoded from hippocampal patterns. a, Decoding accuracy of scripted narrative type from neural patterns. The vertical black line denotes decoding accuracy of ground-truth script type ('PTSD' versus 'Sad') from hippocampal spatial patterns in the empirical condition. The colored histogram is a surrogate distribution comprising decoding accuracy for the same neural data with shuffled labels. The *P* value is derived nonparametrically through a two-sided permutation test ($n = 2{,}500$, $P = 0.0028$). **b**, Same as **a** but for decoding accuracy of 'PTSD' versus 'Calm' from hippocampal spatial patterns ($n = 2{,}500$, $P = 0.0004$). **c**, Same as **a** but for decoding accuracy of 'PTSD' versus 'Sad' from amygdala spatial patterns ($n = 2{,}500$, $P = 0.097$). **d**, Same as **a** but for decoding accuracy of 'PTSD' versus 'Calm' from amygdala spatial patterns ($n = 2{,}500$, $P = 0.002$).

with higher hippocampal IS-RSA values ('Calm': mean 'lowest' = −0.142, 'highest' = 0.026, two-sample Student's *t*-test $t(198) = -3.21$, $P = 0.0015$; 'Sad: mean 'lowest' = 0.067, 'highest' = 0.219, two-sample Student's *t*-test $t(198) = -3.22$, $P = 0.0014$; Supplementary Fig. 11a,b). Conversely, 'PTSD' scripts exhibited an opposite effect where higher semantic similarity was significantly associated with lower hippocampal IS-RSA ('PTSD: mean 'lowest' = 0.069, 'highest' = −0.171, two-sample Student's *t*-test $t(198) = 5.09$, $P = 6.14 \times 10^{-7}$; Supplementary Fig. 11c).

The same analysis conducted on PCC patterns showed a consistent and robust link between semantic similarity and neural similarity, regardless of script type ('Calm': mean 'lowest' = −0.306, 'highest' = 0.052, two-sample Student's *t*-test $t(198) = -8.97$, $P = 2.31 \times 10^{-16}$; 'Sad: mean 'lowest' = −0.044, 'highest' = 0.513, two-sample Student's *t*-test $t(198) = -13.08$, $P = 1.41 \times 10^{-28}$; 'PTSD: mean 'lowest' = −0.051, 'highest' = 0.382, two-sample Student's *t*-test $t(198) = -7.49$, $P = 2.24 \times 10^{-12}$; Supplementary Fig. 11d–f). See Supplementary Table 3 for a detailed summary of central tendency measurements for this analysis.

Involvement of hippocampal subregions in representation

Evidence suggests that hippocampal subregions along its longitudinal axis are recruited differently during tasks involving recall autobiographical memory and scene construction[48,49], with particular implications in PTSD[50–52]. With this in mind, we conducted an exploratory analysis to further delineate the differences in patterns of hippocampal representation of traumatic autobiographical memory narratives. We conducted IS-RSA on neural patterns extracted separately from the anterior and posterior extremities of the hippocampus (split into three segments: anterior, middle and posterior; Methods).

We observed that the semantic representations tended to be more pronounced in the posterior part of the hippocampus (posterior hippocampus: 'PTSD', $\rho = -0.0506$, $P = 0.327$; 'Sad', $\rho = 0.169$, $P_{(\text{FDR-corrected})} = 0.0004$; coefficient comparison (two-tailed) 'PTSD' versus 'Sad', $P_{(\text{FDR-corrected})} = 0.0005$; anterior hippocampus: 'PTSD', $\rho = -0.0503$, $P = 0.329$; 'Sad', $\rho = 0.065$, $P = 0.204$; coefficient comparison (two-tailed) 'PTSD' versus 'Sad', $P = 0.112$; Supplementary Fig. 12). When tested directly, the difference between the correlation coefficients was not significant ($P = 0.141$).

Memory type can be decoded from hippocampal patterns

To further support our finding that hippocampal neural patterns were linked to the semantic content of the autobiographical memories in 'Sad', but not in 'PTSD', script reactivation, we sought a complementary

https://doi.org/10.1038/s41593-023-01483-5

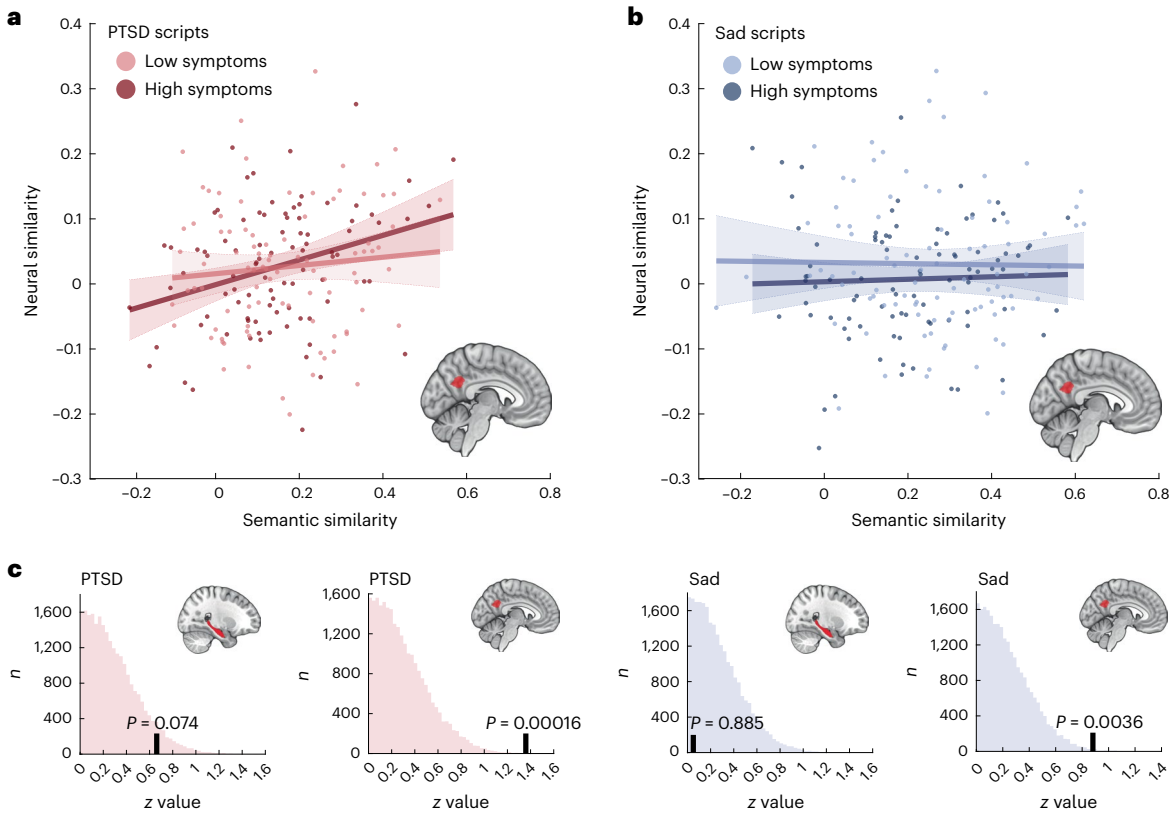

Fig. 5 | Symptom severity modulates PCC representation of PTSD memory. **a**, IS-RSA in the PCC differed by symptom severity. IS-RSA was conducted on pairwise similarity of the semantic content of 'PTSD' narratives and neural patterns in the PCC on subgroups differing in symptom severity (low and high). Each datapoint is derived from a pairwise comparison. Analysis was iterated per subgroup. Regression lines are approximate visualization of Spearman's correlation ρ coefficients for IS-RSA in low and high symptoms (light and dark red, respectively). Error bands indicate 95% CIs. **b**, Same as **a** but conducted on semantic content of 'Sad' narratives and neural patterns in the PCC on subgroups differing in symptom severity (low and high are light and dark blue, respectively). Error bands indicate 95% CIs. **c**, Permutation test for differences in IS-RSA by symptom severity. The vertical black line denotes z-transformed difference (high−low) in correlation coefficients in semantic-to-neural IS-RSA. The colored histogram is a surrogate distribution comprising randomly generated shuffled severity labels. The P value is derived nonparametrically via a permutation test, uncorrected (n = 25,000). From left to right: hippocampal patterns during 'PTSD' narratives (z = 0.661, P = 0.074). The PCC patterns are shown during 'PTSD' narratives (z = 1.359, P = 0.00016), the hippocampal patterns during 'Sad' narratives (z = 0.05, P = 0.885) and the PCC patterns during 'Sad' narratives (z = 0.881, P = 0.0036).

approach by which these two conditions could be teased apart. With this in mind, we trained a regularized linear discriminant analysis (rLDA) model to decode narrative conditions ('PTSD' or 'Sad') from the multivoxel spatial patterns extracted from the hippocampus during script reactivation. Using 25-fold crossvalidation, we were able to decode at 66.2% accuracy for whether hippocampal spatial patterns belonged to a 'PTSD' or a 'Sad' narrative. To assess the power of this predictive ability, we iterated the procedure with shuffled labels (n = 2,500) to obtain a surrogate distribution of decoding accuracy (mean ± s.d. = 52.7% ± 4.9%). Nonparametric testing confirmed that decoding accuracy for the empirical data was well above chance (P = 0.0028; Fig. 4a). To further validate our finding, we then attempted to decode 'PTSD' from 'Calm' scripts, expecting those to be teased apart more easily given their different mental state. Indeed, we were able to decode these conditions at 80.9% accuracy, which was well above chance (mean ± s.d. = 54.2% ± 5.0%, P < 0.0001; Fig. 4b). For comparison, spatial patterns derived from the amygdala could not be used as robustly to distinguish between 'PTSD' and 'Sad' scripts (decoding accuracy for empirical data: 58.2%, surrogate: mean ± s.d. = 52.2% ± 4.7%, P = 0.097; Fig. 4c,d). These findings provide additional support for the idea that hippocampal activity during traumatic autobiographical memory recall represents elements of the narrative and these patterns are observably different from activity during nontraumatizing autobiographical memory recall.

Symptom level modulates PCC representation of PTSD memory

Having observed that similar nontraumatic semantic content is associated with similar neural patterns in the hippocampus, but not in the PCC, we asked whether individual differences in PTSD symptom severity may have attenuated the group effects observed through IS-RSA. We therefore carried out an exploratory analysis in which we asked whether PTSD severity, operationalized as a CAPS for DSM-5 (CAPS-5) score evaluated during screening, will explain the between-subject variability to the extent by which narratives will be represented in the PCC. To this end, we split the cohort into two subgroups (both n = 14) labeled 'high' and 'low' according to the median of their CAPS-5 score. The total scores in the study ranged between 26 and 60 (mean ± s.d. = 41.2 ± 8.3). Setting a cutoff CAPS-5 score of 38 (noninclusive), the two resulting subgroups significantly differed in their CAPS-5 score ('high' = 47.8 ± 3.4, 'low' = 34.7 ± 6.5; t(26) = 6.68, P < 0.0001).

First, we verified that univariate BOLD responses in these ROIs were comparable. We used a whole-brain, two-sample Student's t-test design to compare the 'high' and 'low' symptom groups' response across script types. In both 'PTSD' > 'Calm' and 'PTSD' > 'Sad' contrasts, we were not able to detect differences between the groups using cluster size threshold corrected with a family-wide error rate of $P_{(FWE)}$ < 0.05. Next, we verified that semantic similarity within these subgroups was comparable, that is, that script similarity within each script category did not differ between the groups.

The rmANOVA uncovered a main effect of script type ($F(2, 180) = 108.56$, $P < 0.00001$), a main effect of 'symptom severity' ($F(1, 90) = 11.02$, $P = 0.00131$) but no interaction between the two ($F(2, 180) = 2.15$, $P = 0.119$). Post hoc comparisons (Bonferroni corrected) revealed that, in 'PTSD' and 'Sad' scripts, the average semantic similarity did not differ between the high and low symptom groups (two-sample Student's t-test, $t(180) = -0.73$, $P = 1$; $BF_{10} = 0.207$; 'Sad': $t(180) = -2.03$, $P = 0.22$, $BF_{10} = 1.09$). In the 'Calm' condition, script similarity was significantly higher in the low group than in the high one ('Calm': $t(180) = -3.18$, $P = 0.0043$, $BF_{10} = 16.23$). We therefore applied ensuing IS-RSA only to the 'PTSD' and 'Sad' conditions.

We conducted IS-RSA separately for each subgroup, using its corresponding semantic and neural similarity matrices. Matrix dimensions were 14 × 14, which, when vectorized, resulted in 91 values. We compared the resulting Spearman's coefficients that were derived for each of the two symptom groups using a nonparametric test. We split the full cohort into two random subgroups iteratively ($n = 25{,}000$) and computed a surrogate distribution to which the statistics of the true, CAPS-5-based split were compared.

The PCC displayed a strong discriminative utility where higher symptom severity was associated with stronger semantic representation of 'PTSD' scripts (Fig. 5a). Representation of the 'Sad' scripts also showed stronger representation in the high symptom group, but to a much lesser extent (Fig. 5b) (PCC 'PTSD': high: $\rho = 0.266$; low: $\rho = 0.0687$; 'Sad': high: $\rho = 0.0756$; low: $\rho = -0.0537$). In tandem with the functional ROI, the PCC was also defined anatomically in two supporting ROI analyses to account for the ROI definition method (Methods and Supplementary Fig. 13)

By contrast, in the hippocampus, the extent of the link between neural patterns and semantic representations of both 'PTSD' and 'Sad' scripts did not differ by symptom severity (hippocampus 'PTSD': high: $\rho = -0.254$; low: $\rho = -0.163$; 'Sad': high: $\rho = 0.199$; low: $\rho = 0.206$). Nonparametric permutation tests asserted that the Spearman's coefficients differed significantly by symptom severity in the IS-RSA based on the PCC, but not the hippocampal neural patterns (PCC 'PTSD': coefficient difference$_{(high-low)} = 0.197$, nonparametric permutations $P_{(FDR\ corrected)} = 0.001$; 'Sad': coefficient difference$_{(high-low)} = 0.129$, nonparametric permutations $P_{(FDR\ corrected)} = 0.011$; hippocampus 'PTSD': coefficient difference$_{(high-low)} = -0.074$, nonparametric permutations $P_{(FDR\ corrected)} = 0.875$; 'Sad': coefficient difference$_{(high-low)} = -0.007$, nonparametric permutations $P_{(FDR\ corrected)} = 0.885$) (Fig. 5c).

We further observed that symptom severity modulation of the link between neural patterns and semantic representations of 'PTSD', but not 'Sad', scripts was specific to the PCC and did not extend into the amygdala ('PTSD': high: $\rho = 0.037$; 'low: $\rho = -0.082$; 'Sad': high: v = 0.054; low: $\rho = 0.120$; PTSD: coefficient difference$_{(high-low)} = 0.1184$, nonparametric permutations $P_{(FDR\ corrected)} = 0.02$; note that this effect is driven by the small negative correlation in the low condition; 'Sad': coefficient difference$_{(high-low)} = -0.0657$, nonparametric permutations $P_{(FDR\ corrected)} = 0.286$) (Supplementary Fig. 14).

This result suggests that the severity of PTSD symptoms is linked to the semantic representation of the traumatic narrative in the PCC but not in the amygdala, whereas the differentiation in representation observed in the hippocampus persisted regardless of symptom severity.

Discussion

Despite continuous effort, the nature of intrusive traumatic autobiographical memories and the mechanisms underlying their unique perceptual attributes in PTSD remain largely unknown[53]. In the present study, we used individualized traumatic autobiographical memory narratives in a script reactivation paradigm, in which patients with PTSD listened to a new rendition of their traumatic memory. We set out to ask whether, and how, the hippocampus, amygdala and PCC differentiate traumatic autobiographical memories from sad ones. Given the duration and richness of the stimuli, our paradigm was at the intersection of autobiographical memory reactivation and naturalistic narrative comprehension tasks.

We leveraged the variance between idiosyncratic memories by quantifying their semantic similarity to ask whether their neural representations are altered during the processing of personal trauma narratives, compared with negative nontraumatic narratives of the same individuals ('Sad'). Using IS-RSA, we found that hippocampal patterns showed a differentiation in semantic representation by narrative type; 'Sad' scripts that were semantically similar (for example, death of a loved one) across participants elicited similar neural representations. Conversely, thematically similar traumatic autobiographical memories (of the DSM-5 Criterion A event) did not elicit similar representations. Unlike the hippocampus, the amygdala did not represent semantic information in a notable manner, suggesting a poorer representational space for semantic content.

Finally, in an exploratory analysis, we focused on the PCC to ask whether, unlike the hippocampus, this region—recently conceptualized as a cognitive bridge between world events and representation of the self[33,54]—will demonstrate a positive relationship between semantic content and neural patterns of the traumatic narratives. We did indeed observe such a relationship in the PCC, with individual symptom severity mediating the extent of semantic-to-neural representation. Conversely, this differentiation by PTSD severity was not evident in the hippocampus. An exploratory analysis did not reveal any additional regions of the DMN evincing the same function.

Semantic-to-neural mapping has been demonstrated comprehensively, in both the hippocampus[55–57] and the cortex[58,59]. Therefore, we expected to observe a link between narratives' semantic similarity and elicited neural similarity. That said, in the present study we make two advances: first, we extended this understanding into an underexplored domain—real-life traumatic autobiographical memories in PTSD; and, second, we observed that, within the same brains, hippocampal representations differed considerably between two types of autobiographical memory of comparable content and valence.

In a complementary approach, we decoded condition identity from the hippocampal patterns. The fact that we were able to tease the two negative conditions apart suggests that these signals hold some shared high-dimensional pattern, implying a common cognitive state shared across participants.

Our key findings therefore are twofold: first, that the emotional content of autobiographical memories is represented differently in the two major systems subserving autobiographical memory—the hippocampus and the PCC; and, second, that traumatic autobiographical memories undergo a parallel or dissociable mode of representation, suggesting that they profoundly differ from neurotypical autobiographical memories of comparable content and valence.

Why would traumatic autobiographical memories be represented differently to nontraumatic ones? We discuss several explanations: patients with PTSD may develop a highly detailed and very personal memory of their traumatic event and thus their semantic representations become highly idiosyncratic (that is, unique to the individual). This interpretation is in line with a recent study[60] reporting that the more concepts perceived as self-relevant, the more person-specific became their neural representation of valence. Thus, it is possible that PTSD phenomenology generates an overly personal autobiographical memory, which, despite being semantically similar to other memories, is linked to highly idiosyncratic representations. Another possibility is that traumatic memory reactivation is not experienced as memory as such, but is rather disconnected from time and space and from current surroundings, and thus experienced as an intrinsic mental event, akin to the internal processing that typically engages the DMN.

Last, an intriguing possibility is that patients attempted to block or suppress the reactivation of the traumatic content and, by doing so, exhibited brain activity that was incongruent with the semantic content

presented to them[61,62]. Re-examining the nature of these memories after successful trauma-focused psychotherapy may shed further light on the observed results.

In clinical settings, the evaluation of traumatic memory organization is often reliant mostly on meta-memory: the patient's self-report about memory coherence and meaning of the traumatic experience[63]. Semantic representation of idiosyncratic autobiographical memories using IS-RSA may allow a more objective neural marker for PTSD. For example, we may observe the emergence of semantic-to-neural mapping of the traumatic memory within the hippocampus in the course of treatment. Trauma-focused psychotherapy could help restore a narrative and also align the narrative with a more normative and less idiosyncratic meaning.

Finally, we would like to acknowledge several limitations of our study: the sample size of 28 patients may have limited the generalizability of the results. This was particularly evident in the ad-hoc analysis involving symptom severity, where the sample was split into two halves. Furthermore, despite the careful construction and thorough analysis of the memory scripts, differences not accounted for may have remained, particularly given their naturalistic nature. For example, we found that the variance of the 'Calm' scripts dataset was low, probably obscuring the semantic-to-neural relationship. Last, our within-subject design, where the traumatic narratives were compared with sad ones within the same individuals, controlled for potential between-cohort effects such as the global alterations in brain structure and connectivity in PTSD. Still, it would be interesting to further delineate the factors that influence semantic-to-neural mapping of autobiographical memories within the neurotypical range, such as parametrically modulating relevancy to self and narrative coherence.

We end with our initial question about the very nature of PTSD phenomenology: is traumatic memory an extreme case of 'standard' negative emotional processing or a different cognitive entity altogether? Our main finding, that hippocampal patterns of patients with PTSD showed a differentiation in semantic representation by narrative type during memory reactivation, supports the idea of a profoundly separate cognitive experience in the reactivation of traumatic memories. This is consistent with the notion that traumatic memories are not experienced as memories as such. Rather, these are fragments of prior events, subjugating the present moment to evade the comfort of belonging to the past.

Online content

Any methods, additional references, Nature Portfolio reporting summaries, source data, extended data, supplementary information, acknowledgements, peer review information; details of author contributions and competing interests; and statements of data and code availability are available at https://doi.org/10.1038/s41593-023-01483-5.

References

1. Weathers, F. W. et al. The Clinician-Administered PTSD Scale for DSM-5 (CAPS-5): development and initial psychometric evaluation in military veterans. *Psychol. Assess.* **30**, 383–395 (2018).
2. Stevens, J. S. et al. Disrupted amygdala-prefrontal functional connectivity in civilian women with posttraumatic stress disorder. *J. Psychiatr. Res* **47**, 1469–1478 (2013).
3. Davachi, L. Item, context and relational episodic encoding in humans. *Curr. Opin. Neurobiol.* **16**, 693–700 (2006).
4. Ranganath, C. Binding items and contexts: the cognitive neuroscience of episodic memory. *Curr. Dir. Psychol. Sci.* **19**, 131–137 (2010).
5. Ekstrom, A. D. & Ranganath, C. Space, time, and episodic memory: the hippocampus is all over the cognitive map. *Hippocampus* **28**, 680–687 (2018).
6. Milivojevic, B., Varadinov, M., Grabovetsky, A. V., Collin, S. H. P. & Doeller, C. F. Coding of event nodes and narrative context in the hippocampus. *J. Neurosci.* **36**, 12412–12424 (2016).
7. Cohn-Sheehy, B. I. et al. The hippocampus constructs narrative memories across distant events. *Curr. Biol.* **31**, 4935–4945.e7 (2021).
8. Squire, L. R. & Wixted, J. T. The cognitive neuroscience of human memory since H.M. *Annu. Rev. Neurosci.* **34**, 259–288 (2011).
9. Moscovitch, M., Cabeza, R., Winocur, G. & Nadel, L. Episodic memory and beyond: the hippocampus and neocortex in transformation. *Annu Rev. Psychol.* **67**, 105–134 (2016).
10. Scoville, W. B. & Milner, B. Loss of recent memory after bilateral hippocampal lesions. *J. Neurol. Neurosurg. Psychiatry* **20**, 11–21 (1957).
11. Karl, A. et al. A meta-analysis of structural brain abnormalities in PTSD. *Neurosci. Biobehav. Rev.* **30**, 1004–1031 (2006).
12. Jin, C. et al. Abnormalities in whole-brain functional connectivity observed in treatment-naive post-traumatic stress disorder patients following an earthquake. *Psychol. Med.* **44**, 1927–1936 (2014).
13. Miller, D. R. et al. Default mode network subsystems are differentially disrupted in posttraumatic stress disorder. *Biol. Psychiatry Cogn. Neurosci. Neuroimaging* **2**, 363–371 (2017).
14. Elzinga, B. M. & Bremner, J. D. Are the neural substrates of memory the final common pathway in posttraumatic stress disorder (PTSD)? *J. Affect. Disord.* **70**, 1–17 (2002).
15. Brewin, C. R., Gregory, J. D., Lipton, M. & Burgess, N. Intrusive images in psychological disorders: characteristics, neural mechanisms, and treatment implications. *Psychol. Rev.* **117**, 210–232 (2010).
16. Joshi, S. A., Duval, E. R., Kubat, B. & Liberzon, I. A review of hippocampal activation in post-traumatic stress disorder. *Psychophysiology* **57**, e13357 (2020).
17. Cahill, L., Babinsky, R., Markowitsch, H. J. & McGaugh, J. L. The amygdala and emotional memory. *Nature* **377**, 295–296 (1995).
18. Liberzon, I. & Sripada, C. S. The functional neuroanatomy of PTSD: a critical review. *Prog. Brain Res.* **167**, 151–169 (2007).
19. Rauch, S. L. et al. Exaggerated amygdala response to masked facial stimuli in posttraumatic stress disorder: a functional MRI study. *Biol. Psychiatry* **47**, 769–776 (2000).
20. Rauch, S. L. et al. A symptom provocation study of posttraumatic stress disorder using positron emission tomography and script-driven imagery. *Arch. Gen. Psychiatry* **53**, 380–387 (1996).
21. Shin, L. M. et al. Regional cerebral blood flow in the amygdala and medial prefrontal cortex during traumatic imagery in male and female vietnam veterans with PTSD. *Arch. Gen. Psychiatry* **61**, 168–176 (2004).
22. Etkin, A. & Wager, T. D. Functional neuroimaging of anxiety: a meta-analysis of emotional processing in PTSD, social anxiety disorder, and specific phobia. *Am. J. Psychiatry* **164**, 1476–1488 (2007).
23. Kensinger, E. A. & Corkin, S. Two routes to emotional memory: distinct neural processes for valence and arousal. *Proc. Natl Acad. Sci. USA* **101**, 3310–3315 (2004).
24. Phelps, E. A. Human emotion and memory: interactions of the amygdala and hippocampal complex. *Curr. Opin. Neurobiol.* **14**, 198–202 (2004).
25. Fanselow, M. S. & LeDoux, J. E. Why we think plasticity underlying Pavlovian fear conditioning occurs in the basolateral amygdala. *Neuron* **23**, 229–232 (1999).
26. Blair, H. T. & Fanselow, M. S. in *Space, Time and Memory in the Hippocampal Formation* (eds Derdikman, D. & Knierim, J. J.) 465–496 (Springer Vienna, 2014).
27. Davis, P. & Reijmers, L. G. The dynamic nature of fear engrams in the basolateral amygdala. *Brain Res. Bull.* **141**, 44–49 (2018).
28. Brewin, C. R. Re-experiencing traumatic events in PTSD: new avenues in research on intrusive memories and flashbacks. *Eur. J. Psychotraumatol.* **6**, 27180 (2015).

29. Rahman, N. & Brown, A. D. Mental time travel in post-traumatic stress disorder: current gaps and future directions. *Front. Psychol.* **12**, 624707 (2021).
30. Rubin, D. C., Boals, A. & Berntsen, D. Memory in posttraumatic stress disorder: properties of voluntary and involuntary, traumatic and nontraumatic autobiographical memories in people with and without posttraumatic stress disorder symptoms. *J. Exp. Psychol. Gen.* **137**, 591–614 (2008).
31. Brewin, C. R. Coherence, disorganization, and fragmentation in traumatic memory reconsidered: a response to Rubin et al. (2016). *J. Abnorm. Psychol.* **125**, 1011–1017 (2016).
32. Foa, E. B., Molnar, C. & Cashman, L. Change in rape narratives during exposure therapy for posttraumatic stress disorder. *J. Trauma Stress* **8**, 675–690 (1995).
33. Yeshurun, Y., Nguyen, M. & Hasson, U. The default mode network: where the idiosyncratic self meets the shared social world. *Nat. Rev. Neurosci.* **22**, 181–192 (2021).
34. Andrews-Hanna, J. R., Saxe, R. & Yarkoni, T. Contributions of episodic retrieval and mentalizing to autobiographical thought: evidence from functional neuroimaging, resting-state connectivity, and fMRI meta-analyses. *NeuroImage* **91**, 324–335 (2014).
35. Golland, Y. et al. Extrinsic and intrinsic systems in the posterior cortex of the human brain revealed during natural sensory stimulation. *Cereb. Cortex* **17**, 766–777 (2007).
36. Simony, E. et al. Dynamic reconfiguration of the default mode network during narrative comprehension. *Nat. Commun.* **7**, 12141 (2016).
37. Sambuco, N., Bradley, M. M. & Lang, P. J. Narrative imagery: emotional modulation in the default mode network. *Neuropsychologia* **164**, 108087 (2022).
38. Akiki, T. J., Averill, C. L. & Abdallah, C. G. A network-based neurobiological model of PTSD: evidence from structural and functional neuroimaging studies. *Curr. Psychiatry Rep.* https://doi.org/10.1007/s11920-017-0840-4 (2017).
39. Koch, S. B. J. et al. Aberrant resting-state brain activity in posttraumatic stress disorder: a meta-analysis and systematic review. *Depress. Anxiety* **33**, 592–605 (2016).
40. Boccia, M. et al. Different neural modifications underpin PTSD after different traumatic events: an fMRI meta-analytic study. *Brain Imaging Behav.* **10**, 226–237 (2016).
41. Kozlowski, A. C., Taddy, M. & Evans, J. A. The geometry of culture: analyzing the meanings of class through word embeddings. *Am. Sociol. Rev.* **84**, 905–949 (2019).
42. Van Uden, C. E. et al. Modeling semantic encoding in a common neural representational space. *Front. Neurosci.* **12**, 437 (2018).
43. Zhang, Y., Han, K., Worth, R. & Liu, Z. Connecting concepts in the brain by mapping cortical representations of semantic relations. *Nat. Commun.* **11**, 1877 (2020).
44. Solomon, E. A., Lega, B. C., Sperling, M. R. & Kahana, M. J. Hippocampal theta codes for distances in semantic and temporal spaces. *Proc. Natl Acad. Sci. USA* **116**, 24343–24352 (2019).
45. Mikolov, T., Chen, K., Corrado, G. & Dean, J. Efficient estimation of word representations in vector space. Preprint at https://arxiv.org/abs/1301.3781 (2013).
46. Mantel, N. The detection of disease clustering and a generalized regression approach. *Cancer Res.* **27**, 209–220 (1967).
47. Nummenmaa, L. et al. Emotional speech synchronizes brains across listeners and engages large-scale dynamic brain networks. *NeuroImage* **102**, 498–509 (2014).
48. Strange, B. A., Witter, M. P., Lein, E. S. & Moser, E. I. Functional organization of the hippocampal longitudinal axis. *Nat. Rev. Neurosci.* **15**, 655–669 (2014).
49. Poppenk, J., Evensmoen, H. R., Moscovitch, M. & Nadel, L. Long-axis specialization of the human hippocampus. *Trends Cogn. Sci.* **17**, 230–240 (2013).
50. Abdallah, C. G. et al. Anterior hippocampal dysconnectivity in posttraumatic stress disorder: a dimensional and multimodal approach. *Transl. Psychiatry* **7**, e1045–e1047 (2017).
51. Malivoire, B. L., Girard, T. A., Patel, R. & Monson, C. M. Functional connectivity of hippocampal subregions in PTSD: relations with symptoms. *BMC Psychiatry* **18**, 129 (2018).
52. Satpute, A. B., Mumford, J. A., Naliboff, B. D. & Poldrack, R. A. Human anterior and posterior hippocampus respond distinctly to state and trait anxiety. *Emotion* **12**, 58–68 (2012).
53. Lanius, R. A. et al. The nature of traumatic memories: a 4-T fMRI functional connectivity analysis. *Am. J. Psychiatry* **161**, 36–44 (2004).
54. Raichle, M. E. The brain's default mode network. *Annu. Rev. Neurosci.* **38**, 433–447 (2015).
55. Viganò, S. & Piazza, M. Distance and direction codes underlie navigation of a novel semantic space in the human brain. *J. Neurosci.* **40**, 2727–2736 (2020).
56. Morton, N. W., Zippi, E. L., Noh, S. M. & Preston, A. R. Semantic knowledge of famous people and places is represented in hippocampus and distinct cortical networks. *J. Neurosci.* **41**, 2762–2779 (2021).
57. Brunec, I. K., Robin, J., Olsen, R. K., Moscovitch, M. & Barense, M. D. Integration and differentiation of hippocampal memory traces. *Neurosci. Biobehav. Rev.* **118**, 196–208 (2020).
58. Huth, A. G., De Heer, W. A., Griffiths, T. L., Theunissen, F. E. & Gallant, J. L. Natural speech reveals the semantic maps that tile human cerebral cortex. *Nature* **532**, 453–458 (2016).
59. Patterson, K., Nestor, P. J. & Rogers, T. T. Where do you know what you know? The representation of semantic knowledge in the human brain. *Nat. Rev. Neurosci.* **8**, 976–987 (2007).
60. Kim, B., Andrews-Hanna, J. R., Han, J., Lee, E. & Woo, C.-W. When self comes to a wandering mind: brain representations and dynamics of self-generated concepts in spontaneous thought. *Sci. Adv.* **8**, eabn8616 (2022).
61. Anderson, M. C. et al. Neural systems underlying the suppression of unwanted memories. *Science* **303**, 232–235 (2004).
62. Anderson, M. C. & Levy, B. J. Suppressing unwanted memories. *Curr. Dir. Psychol. Sci.* **18**, 189–194 (2009).
63. Bedard-Gilligan, M., Zoellner, L. A. & Feeny, N. C. Is trauma memory special? Trauma narrative fragmentation in ptsd: effects of treatment and response. *Clin. Psychol. Sci.* **5**, 212–225 (2018).

Methods

Experimental paradigm

The present study was registered at clinicaltrials.gov (NCT02727998T) and approved by the Yale University Institutional Review Board. Twenty-eight participants (mean age = 38.1 ± 10.5 years, range = 24–63 years; females (n = 11) and males (n = 17)) took part in the present study after providing a statement of informed consent. All participants had chronic PTSD (see Supplementary Table 2 for cohort demographics). PTSD diagnosis was established using CAPS-5 (ref. 1). The cohort in the present study is part of a larger, longitudinal study focused on the effects of ketamine-aided extinction in PTSD, for which the participants were compensated by a total sum of up to US$700 for their participation in the original clinical trial. Our data are based on the baseline session assessment only, with no drugs being administered. Therefore, blinding was not relevant and data collection and analysis were not performed blind to the conditions of the experiments. No statistical methods were used to predetermine sample sizes, but our sample sizes are similar to those reported in the publication of the aforementioned longitudinal study[64]. Exclusion criteria included a diagnostic history of bipolar disorder, borderline personality disorder, obsessive–compulsive disorder, schizophrenia or schizoaffective disorder, dementia, current psychotic features, suicide risk, moderate or higher severity of substance use disorder and history of traumatic brain injury. Participants who were currently engaged in trauma focus therapy were also ineligible to participate in the study. Last, patients were excluded for acute medical illness. Psychotic features were determined by the Structured Clinical Interview for DSM-IV[65]. All participants who were prescribed psychiatric medication had to maintain a stable dose for 4 weeks before the assessment of PTSD and other study inclusion/exclusion criteria. Therefore, if they met PTSD diagnosis, this was established even in the presence of medication. Randomization was handled by the Yale Investigational Drug Services and participants were randomized in counterbalanced blocks of ten subjects, each stratified by gender.

Of the 28-patient cohort mentioned, no data exclusions were made. All script-reactivation blocks were included in the IS-RSA. Exclusion of specific words from script content is detailed in 'Semantic analysis'.

We used the Sinha method—a previously established, script-driven imagery, development method of autobiographical events, which has been developed as a way to personalize stimuli that induce traumatic imagery and has been widely used as a method of memory reactivation in PTSD research[66–70]. The method aims to produce ecologically valid audio narratives by activating comparable physiological, subjective and behavioral responses across patients. This methodology allows comparison across scripts and across subjects while avoiding confounds such as length, vocabulary, sentence structure and experiential features. The narrative is built based on several hours of clinical sessions, in which patients were asked to describe the events in as much detail as possible. It employs a structured form that is similar across scripts but at the same time highly detailed with specifics (for example, military jargon, nicknames, personal slang) to provoke the individualized experience.

Specifically, patients completed an imagery-development procedure in which they were asked to describe the traumatic event associated with their PTSD, as well as a major sad, but not traumatizing, event ('Sad') and a positive, low-arousal event in which they felt relaxed (referred to as 'Calm'). The imagery scripting procedure followed a procedure presented in ref. 71. Participants were asked to describe the events in as much detail as possible. They were then asked to select at least three physiological responses corresponding to each specific event to be later embedded in the narrative. Using this information, we developed audio scripts, approximately 120-s long for each event (duration: 'PTSD' = 120.19 ± 1.20 s; 'Sad' = 119.64 ± 1.48 s; 'Calm' = 118.69 ± 2.72 s), narrated by a male member of the research staff. The narratives were all in second-form pronouns ('you'/'your'), mostly in the present tense.

The scripts comprised three main elements: the episodic unfolding of events (time and place, scenery description, actions, dialogues), description of mental state (for example, 'you feel helpless', 'a feeling of peace comes over you') and a vocabulary of sensory and somatic phrases used to promote re-experiencing (for example, 'your heart beats faster'). The somatic vocabulary consisted of references to heartbeat, respiration, muscle tone, perspiration, tearing, and so on. Both negatively valenced script types—'PTSD' and 'Sad'—were conveyed using the same vocabulary, to control and maximize the similarity of reactivation between these conditions. The positive scripts ('Calm') often mentioned similar autonomic functions, but with opposite reactions (for example, muscle relaxation, slow breathing).

Semantic analysis

For the purpose of semantic analysis some names, for example, places with greater geographical resolution than a US state, commercial brands or firms and specialized military jargon or acronyms, were removed. Sentences were defined according to full stops, question marks and exclamation marks as they appear in the text read by the narrator. As part of the reactivation procedure aimed to heighten autonomic arousal, the pace (words per script) of both negatively valenced scripts was intentionally higher and their duration slightly longer than the 'Calm' ones.

During preprocessing of the semantic input, punctuation marks were erased, texts were transformed to lower case and tokenized. Stop words, defined by MATLAB R2020a's default natural language processing (NLP) vocabulary, were removed. Words underwent lemmatization and were then assigned a 300-dimension vector representation. The semantic space we used was a pretrained embedding for one million English words (16-B tokens) available through MATLAB's word2vec NLP tools. Vector representations were calculated for each single word. Words in the scripts that were not indexed in the pretrained space were not included in the analysis. The semantic representation of the next level in text hierarchy—the sentence—was calculated as the average representation of the words in it. Similarly, the semantic representation of each entire script was calculated by averaging the representation of its sentences.

In addition, we carried out the same analytical pipeline using a pretrained contextual embedding transformer model, BERT, implemented in the MATLAB R2021a NLP toolbox. Briefly, contextual embedding departs from static semantic representations by being able to account for intrasentence dynamics. As such, in the present study the first level of data input in the hierarchy was sentences, not individual words. Again, representation of scripts was calculated by averaging the representation of its sentences. For both methods, before computing similarity between scripts, we scaled the vector representations by subtracting the average norm of all words embedding in the entire vocabulary used in the study (based on all script types), following a normalization procedure described in ref. 72. The semantic similarity was derived from a transformed distance matrix of pairwise cosine distances of the vectorial representations. We used cosine distance as it is considered to be a better fit for semantic analysis than Euclidean distance because it does not consider vector magnitude, which is often biased in datasets involving text corpora resulting from differences in word occurrence[73,74].

Linguistic evaluation of script content

We applied a series of validations to script content using external psycholinguistic rating databases. We focused on factors that may act as possible confounders in subsequent neural investigation, with specific attention to comparisons between the two negative script types: 'PTSD' and 'Sad'. The following measures were tested: (1) concreteness ratings from the database by Brysbaert et al.[75], which was defined as the

degree to which a concept refers to a perceptible entity; (2) imageability ratings from the Glasgow Norms database by Scott et al.[76], defined as the degree of effort involved in generating a mental image; and (3) valence ratings derived from NRC-VAD, a database by Mohammad et al. which was defined as a position of concept on dimensions of positiveness–negativeness/pleasure–displeasure[77].

Dimensionality reduction

Dimensionality reduction of the semantic information was done using *t*-SNE[78]. Similar to principal component analysis (PCA), *t*-SNE also reduces dimensionality of the input dataset. It is superior, however, to PCA, in its ability to preserve local structure. Projection of *t*-SNE clusters to 3D space was carried out in MATLAB, with an intermediate step of a PCA into 100 components. The learning rate was set to 1,000 and perplexity to 30.

Experimental procedure

All participants listened to each script type three times in the scanner. Participants were naive to this new scripted rendition of their autobiographical memories and not familiar with the voice of the narrator. The order of scripts was fixed and identical across all participants but one. The order was: T–C–S–C–T–S–C–T–S (T = trauma, S = sad, C = calm) in all scans but one, the order of which was S–C–T–C–S–T–C–S–T. The fixed order reflects constraints on the methodology of script reactivation: the need to avoid random back-to-back presentation of two identical scripts to prevent habituation, as well as the need to never end with the trauma script for the sake of the patient's wellbeing after the scan. The predefined sequence factored in all these considerations. Scripts were presented in the scanner using E-prime 2. Each script began with a slide instructing the participant to press a button to initiate the next playback and its type. No visual information was displayed during script playback.

MRI

Magnetic resonance imaging (MRI) data were collected with a Siemens 3-T Prisma scanner, using a 32-channel receiver array head coil. High-resolution structural images were acquired by Magnetization-Prepared Rapid Gradient-Echo imaging (repetition time (TR) = 1 s, time to echo = 2.77 ms, inversion time = 900 ms, flip angle = 9°, 176 sagittal slices, voxel size = $1 \times 1 \times 1$ mm^3, 256×256 matrix in a 256-mm field of view). The fMRI scans were acquired while the participants were listening to the narrated scripts, using a multi-band echo-planar imaging sequence (multi-band factor = 4, TR = 1 s, time to echo = 30 ms, flip angle = 60°, voxel size = $2 \times 2 \times 2$ mm^3, 60 2-mm-thick slices, in-plane resolution = 2×2 mm^2, field of view = 220 mm).

MRI preprocessing

Data were preprocessed with fMRIPrep v.20.2.0 (ref. 79). For a complete preprocessing procedure, please refer to the relevant Methods section. Functional images were motion- and slice-time corrected, aligned to T1 anatomical images and then warped to Montreal Neurological Institute and Hospital (MNI) space. Analysis of the functional data included the following regressors: six movement variables (translation and rotation), framewise displacement (FD), the first six anatomical component-based noise correction (CompCor) and the six first discrete cosine regressors. Subsequent preprocessing and statistical contrasts were done using standard statistical parametric mapping (SPM12, Wellcome Department of Imaging Neuroscience) algorithms (fil.ion.ucl.ac.uk/spm) and customized MATLAB R2018b/R2020a/R2021a code.

ROI analysis

Given our previous interest in the function of the amygdala and hippocampus in PTSD, we defined masks for ROI analysis of these structures, bilaterally using the probabilistic Harvard–Oxford atlas[80] thresholded at 25%[81]. In an exploratory analysis, the PCC ROI was defined functionally through a contrast comparing neural activity during narrative playback (all three script types were included) with intertrial interval baseline. After cluster size thresholding with a $P_{(FWE)} < 0.01$, an ROI consisting of 361 voxels was defined. Before ROI analysis, functional images underwent spatial smoothing using a Gaussian kernel of 1-mm full-width at half maximum to enhance a signal-to-noise ratio and classification accuracy[82]. Time courses were extracted from the entire session and were applied with a discrete cosine transform high-pass filter (cutoff of 128 s)[83]. ROI data were then normalized using *z*-score. Spikes in the data, exceeding four times the voxel's s.d., were applied by de-spiking and interpolated using the mean of one TR engulfing each side of the outlier datapoint. In line with previous studies, functional data were shifted 5 s (5 TRs) to account for the delay in the hemodynamic response compared with the audio stimuli[72,84,85]. The segments containing the script narratives were extracted with time indices rounded to include the nearest TR interval to prevent omission of functional data.

Each script was played three times during the scan. To enhance signal to noise in identifying the recurring pattern elicited by the script, the time course for each ROI was averaged across the three repeats of each script. The three repetitions were always considered as a unit and we did not treat them as individual trials. The voxel time course of this average run was collapsed across time to generate a spatial pattern associated with the reactivation of the specific autobiographical memory. This approach also aided in circumventing the slight mismatches in script durations across participants that would have been detrimental for similarity based on temporal fluctuations.

Intersubject representational similarity analysis

To relate the semantic content with neural representation and to determine whether this representation differs in PTSD-related narratives, we conducted an IS-RSA[73,86–88]. The neural similarity matrix was derived from each ROI separately. The semantic similarity matrix was fixed in all analyses (for some analyses it was broken down to smaller matrices, for example, subcohorts differing in symptom severity).

A neural similarity matrix was then generated by calculating pairwise Pearson's correlation for each pair of the 84 scripts. Metrics that are represented as distance by default (rather than similarity) were transformed to similarity using:

$$\text{Similarity} = \frac{1}{1 + \text{Distance}}.$$

As this study comprised 28 participants, who each listened to 3 different scripts, the narrative-based similarity matrices (for example, semantic, acoustic) consisted of the lower triangle of a 28×28 matrix, extracted separately per narrative type ('PTSD', 'Sad', 'Calm'). This corresponded to 378 unique combinations when vectorized ($(28 \times (28 - 1))/2 = 378$). Similarly, trait-based similarity matrices (for example, CAPS) consisted of the lower triangle of a 28×28 matrix, corresponding to 378 unique combinations. Of note, in our design both the neural responses and the naturalistic stimuli varied across individuals.

IS-RSA uses nonparametric Spearman's correlation because it does not assume normal distribution of similarity coefficients of the semantic or neural signals. For other analyses, data distribution was assumed to be normal but this was not formally tested.

We tested the significance of IS-RSA by subjecting *P* values of Spearman's correlation coefficients amassed across ROIs and conditions (for example, 3 ROIs × 3 script types) by using an FDR at $q = 0.05$ implemented in MATLAB R2018a as function 'fdr_bh'.

To compare correlation coefficients between narrative types (for example, 'PTSD' versus 'Sad'), we used two methods depending on the groups' dependency: in cases where one variable is shared (for example, correlation between CAPS and neural similarity in 'PTSD' narratives compared with correlation between the same CAPS data and neural

similarity in 'Sad' narratives), we used the Steiger test[89] as implemented in 'r_test_paired.m' in MATLAB. Briefly, each correlation coefficient is converted into a *z*-score using Fisher's *r*-to-*z* transformation. Next the asymptotic covariance of the estimates is computed and then used in an asymptotic *z*-test. We reported *P* values from a two-tailed probability distribution. In contrast, in cases where the two comparisons had no shared components (for example, correlation between semantic and neural similarity in 'PTSD' narratives and correlation between semantic and neural similarity in 'Sad' narratives), we used the 'corr_rtest' function in MATLAB to convert both correlation coefficients into *z*-scores using Fisher's *r*-to-*z* transformation and calculate their absolute difference. This value was assigned a *P* value from a cumulative normal distribution function ('normcdf' in MATLAB). We reported *P* values from a two-tailed probability distribution.

We included Bayesian paired tests where appropriate, to provide additional information about the evidence in favor of the null hypothesis[90]. A Cauchy prior of 0.707 was used as set in software defaults[91]. The output Bayesian statistic BF_{10}, was interpreted according to standard recommendations by which BF_{10} ranges of 1–3, 3–10 and 10–30 imply anecdotal, substantial or strong evidence, respectively. All Bayesian statistical analyses were conducted in JASP (2019) v.0.11.1 and v.0.16.4. In Bayesian rmANOVA designs, we compared two models: the null model, which suggests no difference between conditions, and the alternative model, 'script', which suggests that scripts do differ from each other. The two models had equal priors ($P(M) = 0.5$). We report the BF_M per model, which quantifies the change from prior odds to posterior odds after the introduction of the evidence (that is, the data), as well as BF_{10} which was fixed to always compare the script model with the null model.

IS-RSA visualization

IS-RSA is usually calculated using nonparametric tests (Spearman's, Kendall's). However, the limitation of Spearman's, being a ranked test, is that it does not yield a regression in the same manner that linear correlations do. Owing to this technical limitation in visualizing the relationship between data matrices in the IS-RSA, we plotted slopes that are computed based on Pearson's correlation. Note that, despite this difference in visualization, throughout the present study the correlation coefficients reported and discussed are Spearman's ρ values.

Longitudinal parcellation of the hippocampus

To date, several definitions for segmentation of the long axis of the human hippocampus exist. We followed a percentile-based segmentation of the hippocampus into three regions along its long axis, described in ref. 49. To avoid discrepancies between boundaries defined by the various segmentation methods, we omitted the medial part from our analyses and focused only on the two extremities: the most anterior and posterior thirds.

Neural GLM and contrasts

We conducted GLM of the functional scans of each participant by modeling the observed BOLD signals and regressors to identify the relationship between the task events and the hemodynamic response. First, functional data underwent spatial smoothing using a 6-mm full-width at half maximum kernel (note that a different kernel was used in IS-RSA). Next, regressors related to all events were created by convolving a train of delta functions representing the sequence of individual events with the default basis function in SPM12, which consists of a synthetic hemodynamic response function composed of two gamma functions. The GLM included three separate regressors for the onset of the three types of scripts: 'PTSD', 'Sad' and 'Calm'. We carried out linear contrasts of parameter estimates to identify effects in each participant. Statistical maps from all participants were then entered into a second-level group analysis to implement a random-effects statistical model. Statistical maps were rendered using MRIcroGL v.1.12.20.

Classification analysis

We decoded narrative conditions ('PTSD' or 'Sad' script) from multivoxel spatial patterns data using an rLDA classifier, 'fitdiscr' function in MATLAB, which shows superior performance over LDA in high-dimensional imaging data that may present issues of multicollinearity and overfitting. Data from all script repeats of the two negatively valenced conditions, along with corresponding condition labels, were used to train the rLDA. Input data consisted of 28 participants × 2 conditions × 3 repeats, yielding 168 samples in total. To test the model's performance on a testing dataset, we iteratively repeated this process with permuted data partitions ($n = 2{,}500$) per ROI and condition and then applied crossvalidation.

Whole-brain investigation

The main contrast used in the whole-brain investigation was 'All Scripts > Baseline' where all script event types (that is, 'PTSD', 'Sad' and 'Calm') were contrasted with the baseline interval between scripts. Statistical inference was made based on whole-brain statistical maps corrected for multiple comparisons using cluster size $P_{(FWE)} < 0.01$ for the identification and extraction of ROIs.

Acoustic similarity analysis

Acoustic similarity of the scripts was computed based on an acoustic landmark envelope. We used a customized MATLAB script, adapted from ref. 92, to extract the analytic envelope of the speech signal filtered within critical bands based on the Bark scale, which is a psychoacoustic measure of loudness.

Subset analysis

We mapped the link between semantic and neural similarity across subsets by iteratively generating five-script subsets of the original cohort and conducted IS-RSA on all possible combinations separately, implemented in 'nchoosek(N,K)'. This procedure was repeated separately per script type. Next, we sorted the subsets by their within-subject semantic similarity and directly compared the values of IS-RSA correlation coefficients of the hundred highest- and lowest-ranking subsets, using a two-sample Student's *t*-test. Values underwent Fisher's *z*-transformation before they were compared.

Symptom severity analysis

CAPS–PTSD diagnosis was established using the CAPS-5 (ref. 1). CAPS was administered within 1 month of the imaging session. The questionnaire data of one participant were missing and were interpolated using the group's mean per questionnaire item.

Additional definitions of PCC ROI

Willard atlas—functional delineation. We used an atlas-derived ROI to generate the PCC mask—the PCC from the Willard functional atlas[93], which is extensively used for a priori demarcation of the PCC. Notably, this was also the ROI in the study by Chen et al.[94] investigating shared memory representations across individuals. Compared with the functionally derived ROI, the Willard atlas ROI is considerably bigger. The Willard–PCC displayed a strong discriminatory utility where higher symptom severity was associated with stronger semantic representation of 'PTSD' scripts. Representation of the 'Sad' scripts also showed stronger representation in the high symptom group, but to a lesser extent (Willard–PCC 'PTSD': high: $\rho = 0.249$; low: $\rho = 0.031$; 'Sad': high: $\rho = 0.182$; low: $\rho = 0.109$; Supplementary Fig. 13a,b). Nonparametric permutation tests asserted that Spearman's coefficients significantly differed by symptom severity in the IS-RSA (PTSD: coefficient difference (high–low) = 0.218, nonparametric permutations $P = 0.00044$; 'Sad': coefficient difference (high–low) = 0.073, nonparametric permutations $P = 0.2476$)

The 4-mm spherical ROI—anatomical center. To further corroborate the contribution of PTSD symptom severity to autobiographical

memory representations in the PCC, we sampled a considerably smaller area of the PCC as well. In the present study we used a 4-mm sphere, sampled from the anatomical center of the PCC. This ROI was obtained from a study by Simony et al. who investigated the role of the DMN in representation of narrative across individuals[36]. The spherical ROI PCC also displayed a strong discriminatory utility, where higher symptom severity was associated with stronger semantic representation of 'PTSD' scripts. Representation of the 'Sad' scripts also showed stronger representation in the high symptom group, but to a lesser extent (spherical ROI PCC: 'PTSD': high: $\rho = 0.293$; low: $\rho = 0.086$; 'Sad': high: $\rho = 0.167$; low: $\rho = 0.066$; Supplementary Fig. 13c,d). Nonparametric permutation tests asserted that Spearman's coefficients significantly differed by symptom severity in the IS-RSA (PTSD: coefficient difference (high−low) = 0.207, nonparametric permutations $P < 0.0001$; 'Sad': coefficient difference (high−low) = 0.101, nonparametric permutations $P = 0.1085$).

The fMRIprep preprocessing

Results included in the present article come from preprocessing performed using fMRIPrep v.20.2.0 (ref. 95), which is based on Nipype v.1.5.1 (ref. 96). Anatomical data preprocessing: a total of one T1-weighted (T1w) image was found within the input BIDS dataset. The T1w image was corrected for intensity nonuniformity using N4BiasFieldCorrection[97], distributed with ANTs v.2.3.3 (ref. 98) and used as T1w reference throughout the workflow. The T1w reference was then skull stripped with a Nipype implementation of the antsBrainExtraction.sh workflow (from ANTs), using OASIS30ANTs as the target template. Brain tissue segmentation of cerebrospinal fluid (CSF), white matter (WM) and gray matter (GM) was performed on the brain-extracted T1w using fast (FSL v.5.0.9)[99]. Volume-based spatial normalization to one standard space (MNI152NLin2009cAsym) was performed through nonlinear registration with antsRegistration (ANTs v.2.3.3), using brain-extracted versions of both the T1w reference and the T1w template. The following template was selected for spatial normalization: ICBM 152 Nonlinear Asymmetrical template v.2009c (ref. 100).

Functional data preprocessing: for each of the BOLD runs found per subject (across all tasks and sessions), the following preprocessing was performed: first, a reference volume and its skull-stripped version were generated using a customized methodology of fMRIPrep. Susceptibility distortion correction was omitted. The BOLD reference was then coregistered to the T1w reference using flirt (FSL v.5.0.9)[101] with the boundary-based registration cost−function[102]. Coregistration was configured with nine degrees of freedom to account for distortions remaining in the BOLD reference. Head-motion parameters with respect to the BOLD reference (transformation matrices and six corresponding rotation and translation parameters) are estimated before any spatiotemporal filtering using mcflirt (FSL v.5.0.9)[101]. BOLD runs were slice-time corrected using 3dTshift from AFNI 20160207 (ref. 103). The BOLD time series (including slice-timing correction when applied) were resampled on to their original, native space by applying the transforms to correct for head motion. These resampled BOLD time series will be referred to as preprocessed BOLD in original space or just preprocessed BOLD. The BOLD time series were resampled into standard space, generating a preprocessed BOLD run in MNI152NLin2009cAsym space. First, a reference volume and its skull-stripped version were generated using a customized methodology of fMRIPrep.

Several confounding time series were calculated based on the preprocessed BOLD: FD, DVARS and three region-wise global signals. FD was computed using two formulations following Power (absolute sum of relative motions) and Jenkinson (relative root mean square displacement between affines)[104,105]. FD and DVARS are calculated for each functional run, both using their implementations in Nipype. The three global signals are extracted within the CSF, the WM and the whole-brain masks. In addition, a set of physiological regressors was extracted to allow for compone nt-based noise correction (CompCor)[106]. Principal components were estimated after high-pass filtering the preprocessed BOLD time series (using a discrete cosine filter with a 128-s cutoff) for the two CompCor variants: temporal (tCompCor) and anatomical (aCompCor). The tCompCor components are then calculated from the top 2% of variable voxels within the brain mask. For aCompCor, three probabilistic masks (CSF, WM and combined CSF + WM) are generated in anatomical space. The implementation differs from that of Behzadi et al.[106] in that, instead of eroding the masks by 2 pixels on BOLD space, the aCompCor masks subtracted a mask of pixels that probably contain a volume fraction of GM. This mask is obtained by thresholding the corresponding partial volume map at 0.05, and it ensures that components are not extracted from voxels containing a minimal fraction of GM. Finally, these masks are resampled into BOLD space and binarized by thresholding at 0.99 (as in the original implementation).

Components are also calculated separately within the WM and CSF masks. For each CompCor decomposition, the k components with the largest singular values are retained, such that the retained components' time series are sufficient to explain 50% of variance across the nuisance mask (CSF, WM, combined or temporal). The remaining components are dropped from consideration. The head-motion estimates calculated in the correction step were also placed within the corresponding confounds file. The confound time series derived from head-motion estimates and global signals were expanded with the inclusion of temporal derivatives and quadratic terms for each[107]. Frames that exceeded a threshold of 0.5-mm FD or 1.5 standardized DVARS were annotated as motion outliers. All resamplings can be performed with a single interpolation step by composing all the pertinent transformations (that is, head-motion transform matrices, susceptibility distortion correction when available and coregistrations to anatomical and output spaces).

Reporting summary

Further information on research design is available in the Nature Portfolio Reporting Summary linked to this article.

Data availability

Data supporting the findings of this present study are deposited at https://osf.io/dc7jb. The Harvard−Oxford atlas is available at https://neurovault.org/collections/262. The Willard atlas is available at https://pyhrf.github.io/manual/parcellation_mask.html. The set of analyses described in the present study was not preregistered.

Code availability

The scripts used for data analysis are available at https://osf.io/dc7jb. The fMRI preprocessing was done in fMRIPrep and analyses were conducted primarily in MATLAB R2018b, R2020a and R2021a (MathWorks).

References

64. Duek, O. et al. Long term structural and functional neural changes following a single infusion of ketamine in PTSD. *Neuropsychopharmacology* https://doi.org/10.1038/s41386-023-01606-3 (2023).
65. First, M. B. & Gibbon, M. in *Comprehensive Handbook of Psychological Assessment, Vol. 2: Personality Assessment* (eds Hilsenroth, M. J. & Segal, D. L.) 134–143 (Wiley, 2004).
66. Lang, P. J., Levin, D. N., Miller, G. A. & Kozak, M. J. Fear behavior, fear imagery, and the psychophysiology of emotion: the problem of affective response integration. *J. Abnorm. Psychol.* **92**, 276–306 (1983).
67. Pitman, R. K., Orr, S. P., Forgue, D. F., de Jong, J. B. & Claiborn, J. M. Psychophysiologic assessment of posttraumatic stress disorder imagery in Vietnam combat veterans. *Arch. Gen. Psychiatry* **44**, 970–975 (1987).

68. Orr, S. P., Metzger, L. J. & Pitman, R. K. Psychophysiology of post-traumatic stress disorder. *Psychiatr. Clin. North Am.* **25**, 271–293 (2002).
69. Brunet, A. et al. Trauma reactivation plus propranolol is associated with durably low physiological responding during subsequent script-driven traumatic imagery. *Can. J. Psychiatry* **59**, 228–232 (2014).
70. Hoge, E. A. et al. Effect of acute posttrauma propranolol on PTSD outcome and physiological responses during script-driven imagery. *CNS Neurosci. Ther.* **18**, 21–27 (2012).
71. Sinha, R. et al. Enhanced negative emotion and alcohol craving, and altered physiological responses following stress and cue exposure in alcohol dependent individuals. *Neuropsychopharmacology* **34**, 1198–1208 (2009).
72. Vodrahalli, K. et al. Mapping between fMRI responses to movies and their natural language annotations. *NeuroImage* **180**, 223–231 (2018).
73. Nguyen, M., Vanderwal, T. & Hasson, U. Shared understanding of narratives is correlated with shared neural responses. *NeuroImage* **184**, 161–170 (2019).
74. Dimsdale-Zucker, H. R. & Ranganath, C. Representational similarity analyses: a practical guide for functional MRI applications. *Handb. Behav. Neurosci.* **28**, 509–525 (2018).
75. Brysbaert, M., Warriner, A. B. & Kuperman, V. Concreteness ratings for 40 thousand generally known English word lemmas. *Behav. Res Methods* **46**, 904–911 (2014).
76. Scott, G. G., Keitel, A., Becirspahic, M., Yao, B. & Sereno, S. C. Glasgow norms: ratings of 5,500 words on nine scales. *Behav. Res. Methods* **51**, 1258–1270 (2019).
77. Mohammad, S. M. Obtaining reliable human ratings of valence, arousal, and dominance for 20,000 English words. In *Proc. 56th Annual Meeting of the Association of Computational Linguistics (Vol. 1, Long Papers)* **1**, 174–184 (2018).
78. Van der Maaten, L. & Hinton, G. Visualizing data using t-SNE. *J. Mach. Learn. Res.* **9**, 2579–2605 (2008).
79. Esteban, O. et al. poldracklab/fmriprep: 1.0.0-rc5. *Zenodo* https://doi.org/10.5281/zenodo.996169 (2017).
80. Desikan, R. S. et al. An automated labeling system for subdividing the human cerebral cortex on MRI scans into gyral based regions of interest. *NeuroImage* **31**, 968–980 (2006).
81. Deuker, L., Bellmund, J. L., Navarro Schröder, T. & Doeller, C. F. An event map of memory space in the hippocampus. *eLife* **5**, e16534 (2016).
82. Op de Beeck, H. P. Against hyperacuity in brain reading: spatial smoothing does not hurt multivariate fMRI analyses? *NeuroImage* **49**, 1943–1948 (2010).
83. Ben-Yakov, A. & Henson, R. N. The hippocampal film editor: sensitivity and specificity to event boundaries in continuous experience. *J. Neurosci.* **38**, 10057–10068 (2018).
84. Chen, J. et al. Accessing real-life episodic information from minutes versus hours earlier modulates hippocampal and high-order cortical dynamics. *Cereb. Cortex* **26**, 3428–3441 (2016).
85. Yeshurun, Y. et al. Same story, different story: the neural representation of interpretive frameworks. *Psychol. Sci.* **28**, 307–319 (2017).
86. Finn, E. S. et al. Idiosynchrony: from shared responses to individual differences during naturalistic neuroimaging. *NeuroImage* **215**, 116828 (2020).
87. Rhoads, S. A. et al. Mapping neural activity patterns to contextualized fearful facial expressions onto callous-unemotional (CU) traits: intersubject representational similarity analysis reveals less variation among high-CU adolescents. *Personal. Neurosci.* **3**, e12 (2020).
88. Chen, P. H. A., Jolly, E., Cheong, J. H. & Chang, L. J. Intersubject representational similarity analysis reveals individual variations in affective experience when watching erotic movies. *NeuroImage* **216**, 116851 (2020).
89. Steiger, J. H. Tests for comparing elements of a correlation matrix. *Psychol. Bull.* **87**, 245–251 (1980).
90. Gliner, J. A., Leech, N. L. & Morgan, G. A. Problems with null hypothesis significance testing (NHST): what do the textbooks say? *J. Exp. Educ.* **71**, 83–92 (2002).
91. Jeffreys, H. *The Theory of Probability* (Oxford Univ. Press, 1998).
92. Oganian, Y. & Chang, E. F. A speech envelope landmark for syllable encoding in human superior temporal gyrus. *Sci. Adv.* **5**, eaay6279 (2019).
93. Shirer, W. R., Ryali, S., Rykhlevskaia, E., Menon, V. & Greicius, M. D. Decoding subject-driven cognitive states with whole-brain connectivity patterns. *Cereb. Cortex* **22**, 158–165 (2012).
94. Chen, J. et al. Shared memories reveal shared structure in neural activity across individuals. *Nat. Neurosci.* **20**, 115–125 (2017).
95. Esteban, O. et al. fMRIPrep: a robust preprocessing pipeline for functional MRI. *Nat. Methods* **16**, 111–116 (2019).
96. Gorgolewski, K. et al. Nipype: a flexible, lightweight and extensible neuroimaging data processing framework in Python. *Front. Neuroinform.* **5**, 13 (2011).
97. Tustison, N. J. et al. N4ITK: improved N3 bias correction. *IEEE Trans. Med. Imaging* **29**, 1310–1320 (2010).
98. Avants, B. B., Epstein, C. L., Grossman, M. & Gee, J. C. Symmetric diffeomorphic image registration with cross-correlation: evaluating automated labeling of elderly and neurodegenerative brain. *Med. Image Anal.* **12**, 26–41 (2008).
99. Zhang, Y., Brady, M. & Smith, S. Segmentation of brain MR images through a hidden Markov random field model and the expectation-maximization algorithm. *IEEE Trans. Med. Imaging* **20**, 45–57 (2001).
100. Fonov, V. et al. Unbiased average age-appropriate atlases for pediatric studies. *NeuroImage* **54**, 313–327 (2011).
101. Jenkinson, M. & Smith, S. A global optimisation method for robust affine registration of brain images. *Med. Image Anal.* **5**, 143–156 (2001).
102. Greve, D. N. & Fischl, B. Accurate and robust brain image alignment using boundary-based registration. *NeuroImage* **48**, 63–72 (2009).
103. Cox, R. W. & Hyde, J. S. Software tools for analysis and visualization of fMRI data. *NMR Biomed.* **10**, 171–178 (1997).
104. Jenkinson, M., Bannister, P., Brady, M. & Smith, S. Improved optimization for the robust and accurate linear registration and motion correction of brain images. *NeuroImage* **17**, 825–841 (2002).
105. Power, J. D. et al. Methods to detect, characterize, and remove motion artifact in resting state fMRI. *NeuroImage* **84**, 320–341 (2014).
106. Behzadi, Y., Restom, K., Liau, J. & Liu, T. T. A component based noise correction method (CompCor) for BOLD and perfusion based fMRI. *NeuroImage* **37**, 90–101 (2007).
107. Satterthwaite, T. D. et al. An improved framework for confound regression and filtering for control of motion artifact in the preprocessing of resting-state functional connectivity data. *NeuroImage* **64**, 240–256 (2013).

Acknowledgements

We thank T. Orederu and Y. Yeshurun for helpful discussions. We also thank A. Ben Yakov and A. Ravia for their advice on analysis and preprocessing. The main source of funding for the present study was provided by: Independent Investigator Grant (no. 23260) from the Brain and Behavior Research Foundation (Institute of Human Relations (IHR)), Clinical Neurosciences Division of the National Center for PTSD (IHR), a private donation from the American Brain Society (IHR) and the Yale Center for Clinical Investigation,

supported by a CTSA grant from the National Center for Advancing Translational Sciences, a component of the National Institutes of Health (NIH). Funding was also provided by the NIH (grant nos. R01MH122611 and R01MH123069) and The Ream Foundation to D.S. The contents of the manuscript are solely the responsibility of the authors and do not necessarily represent the official view of the NIH.

Author contributions

O.P. conceptualized analyses, conducted and interpreted analyses and visualization, wrote the original draft and edited the paper. O.D. collected data, interpreted data analyses and edited the final paper. K.R.K. analyzed the data. C.G. collected data. J.H.K. obtained funding and edited the final paper. I.L. designed the study, interpreted data analyses and cowrote the paper. I.H.R. designed the study, obtained funding, collected data, interpreted the data analyses and cowrote the paper. D.S. conceptualized analyses, interpreted analyses, obtained funding, wrote the original draft and edited the paper.

Competing interests

The authors declare no competing interests.

Additional information

Supplementary information The online version contains supplementary material available at https://doi.org/10.1038/s41593-023-01483-5.

Correspondence and requests for materials should be addressed to Ilan Harpaz-Rotem or Daniela Schiller.

Peer review information *Nature Neuroscience* thanks Choong-Wan Woo and the other, anonymous, reviewer(s) for their contribution to the peer review of this work.

nature portfolio

Corresponding author(s): Ofer Perl

Last updated by author(s): Jun 9, 2023

Reporting Summary

Nature Portfolio wishes to improve the reproducibility of the work that we publish. This form provides structure for consistency and transparency in reporting. For further information on Nature Portfolio policies, see our Editorial Policies and the Editorial Policy Checklist.

Statistics

For all statistical analyses, confirm that the following items are present in the figure legend, table legend, main text, or Methods section.

n/a	Confirmed
☐	☒ The exact sample size (*n*) for each experimental group/condition, given as a discrete number and unit of measurement
☐	☒ A statement on whether measurements were taken from distinct samples or whether the same sample was measured repeatedly
☐	☒ The statistical test(s) used AND whether they are one- or two-sided *Only common tests should be described solely by name; describe more complex techniques in the Methods section.*
☐	☒ A description of all covariates tested
☐	☒ A description of any assumptions or corrections, such as tests of normality and adjustment for multiple comparisons
☐	☒ A full description of the statistical parameters including central tendency (e.g. means) or other basic estimates (e.g. regression coefficient) AND variation (e.g. standard deviation) or associated estimates of uncertainty (e.g. confidence intervals)
☐	☒ For null hypothesis testing, the test statistic (e.g. *F*, *t*, *r*) with confidence intervals, effect sizes, degrees of freedom and *P* value noted *Give P values as exact values whenever suitable.*
☒	☐ For Bayesian analysis, information on the choice of priors and Markov chain Monte Carlo settings
☒	☐ For hierarchical and complex designs, identification of the appropriate level for tests and full reporting of outcomes
☐	☒ Estimates of effect sizes (e.g. Cohen's *d*, Pearson's *r*), indicating how they were calculated

Our web collection on statistics for biologists contains articles on many of the points above.

Software and code

Policy information about availability of computer code

Data collection	Audio-clips were presented during neuroimaging using E-prime 2
Data analysis	Data were preprocessed with Fmriprep, version 20.2.0 and MATLAB R2018b, R2020a and R2022a. Semantic analysis was done with word2vec and BERT within MATLAB. Subsequent preprocessing and statistical contrasts were done using standard statistical parametric mapping (SPM12). Visualization of brain activation was done with MRIcroGL v. 1.12.20. The scripts used for data analysis are available in https://osf.io/dc7jb/

For manuscripts utilizing custom algorithms or software that are central to the research but not yet described in published literature, software must be made available to editors and reviewers. We strongly encourage code deposition in a community repository (e.g. GitHub). See the Nature Portfolio guidelines for submitting code & software for further information.

Data

Policy information about availability of data

All manuscripts must include a data availability statement. This statement should provide the following information, where applicable:

- Accession codes, unique identifiers, or web links for publicly available datasets
- A description of any restrictions on data availability
- For clinical datasets or third party data, please ensure that the statement adheres to our policy

Data supporting the findings of this study are deposited in https://osf.io/dc7jb/.

The Harvard-Oxford atlas is available at https://neurovault.org/collections/262.
The Willard atlas is available at: https://pyhrf.github.io/manual/parcellation_mask.html
The set of analyses described in this study was not preregistered

Human research participants

Policy information about studies involving human research participants and Sex and Gender in Research.

Reporting on sex and gender	Both male and female (self-reported gender) were recruited. No gender-specific effects were investigated in this study. Out of 28 participants, 11 were female. Gender was disclosed by participants during screening.
Population characteristics	Mean age of the cohort was 38.2 ± 10.4 years. All participants had chronic PTSD. PTSD diagnosis was established using the Clinician-Administered PTSD Scale (CAPS-5). Clinician-Administered PTSD Scale for DSM-5 (CAPS-5). A higher score is associated with higher severity of PTSD. The mean CAPS-5 score of the cohort was CAPS score = 41.2 ± 8.3. CAPS scores were used as a covariate to ask whether symptom severity modulate the effects observed in the hippocampal processing of the autobiographical memory.
Recruitment	The subject pool used in the current study data analyses was taken out of a pull of participants which were screened into a clinical trial. As such, rigorous inclusion criteria were applied (as outlined in Duek et al 2023). Thus, the results presented may be limited to eligible study population and cannot be generalized to the entire population of individual diagnosed with PTSD excluded from this original study During the first visit participants underwent a clinical interview to establish a PTSD diagnosis and other eligibility criteria. If found eligible, participants were invited to take part in a 7-day study. The purpose of the longitudinal study is to combine a single infusion of Ketamine with 7-days of trauma focus psychotherapy to relieve post traumatic stress disorder (PTSD) symptoms more effectively. In our analyses we used only data from a baseline imaging session that took place before any drugs were administered.
Ethics oversight	The current study was a secondary data analysis on study which was approved by Yale Institutional Review Board

Note that full information on the approval of the study protocol must also be provided in the manuscript.

Field-specific reporting

Please select the one below that is the best fit for your research. If you are not sure, read the appropriate sections before making your selection.

☒ Life sciences ☐ Behavioural & social sciences ☐ Ecological, evolutionary & environmental sciences

For a reference copy of the document with all sections, see nature.com/documents/nr-reporting-summary-flat.pdf

Life sciences study design

All studies must disclose on these points even when the disclosure is negative.

Sample size	Typically for neuroimaging studies employing a within-subject paradigm, 30 participants is considered a standard sample size. In this case given the limited availability of eligible participants diagnosed with PTSD, we were able to screen only the required sample size of 30 participants. Out of which, 2 were excluded (see below).
Data exclusions	This investigation was part of a larger, longitudinal study. Out of 30 participants that were eligible, 28 were randomized (two did not randomize due to lost contact (this information is reported in CONSORT). Those exclusion criteria due to technical reasons were pre-established.
Replication	The findings reported here were not replicated within the scope of current investigation due to the limited sample size of the patient cohort. We currently aim to replicate these methods on an additional scanning session of a PTSD cohort once it is available.
Randomization	Randomization was handled by the Yale Investigational Drug Services and participants were randomized in counterbalanced blocks of 10-subjects each, stratified by gender
Blinding	This investigation was part of a larger, longitudinal study in which a drug treatment was randomized. We note again that this randomization was not applicable to the subset of data used in this study. The entire study team was blind to the conditions

Reporting for specific materials, systems and methods

We require information from authors about some types of materials, experimental systems and methods used in many studies. Here, indicate whether each material, system or method listed is relevant to your study. If you are not sure if a list item applies to your research, read the appropriate section before selecting a response.

Materials & experimental systems

n/a	Involved in the study
☒	☐ Antibodies
☒	☐ Eukaryotic cell lines
☒	☐ Palaeontology and archaeology
☒	☐ Animals and other organisms
☐	☒ Clinical data
☒	☐ Dual use research of concern

Methods

n/a	Involved in the study
☒	☐ ChIP-seq
☒	☐ Flow cytometry
☐	☒ MRI-based neuroimaging

Clinical data

Policy information about clinical studies

All manuscripts should comply with the ICMJE guidelines for publication of clinical research and a completed CONSORT checklist must be included with all submissions.

Clinical trial registration	NCT02727998
Study protocol	https://clinicaltrials.gov/ct2/show/record/NCT02727998?view=record
Data collection	Data were collected in Yale University School of Medicine New Haven, Connecticut, United States, between the dates December 2015 and November 2021 (Final data collection date for primary outcome measure)
Outcomes	This investigation was part of a larger, longitudinal study. Our study, which used a subset of the data did not have pre-defined clinical outcomes

Magnetic resonance imaging

Experimental design

Design type	Narrative comprehension - block design of listening to audio clips
Design specifications	Blocks (e.g an audio script) were approx. 2 min long. 9 blocks were played, with a self-paced interval between trials that was capped at 10 seconds. Overall duration of the functional scan time was roughly 20 minutes. Other scans (scout, anatomical MPRAGE) took place as well.
Behavioral performance measures	No behavioral measures were recorded. This study looked into implicit brain signals associated with memory reactivation. No performance measures were acquired or logged.

Acquisition

Imaging type(s)	functional, structural
Field strength	3T
Sequence & imaging parameters	High-resolution structural images were acquired by Magnetization-Prepared Rapid Gradient-Echo (MPRAGE) imaging (TR = 1.9 s, TE = 2.77 ms, TI = 900 ms, flip angle = 9°, 176 sagittal slices, voxel size = 1 ×1 × 1 mm, 256 × 256 matrix in a 256 mm FOV).
Area of acquisition	Whole brain

Diffusion MRI ☐ Used ☒ Not used

Preprocessing

Preprocessing software	Data were preprocessed with Fmriprep, version 1.5.6. Smoothing was done post-hoc with SPM, using 1mm and 6mm kernels for spatial patterns and GLM analyses respectively.
Normalization	The T1-weighted (T1w) image was corrected for intensity non-uniformity (INU) with N4BiasFieldCorrection (Tustison et al. 2010), distributed with ANTs 2.3.3 (Avants et al. 2008, RRID:SCR_004757), and used as T1w-reference throughout the workflow. The T1w-reference was then skull-stripped with a Nipype implementation of the antsBrainExtraction.sh workflow (from ANTs), using OASIS30ANTs as target template. Brain tissue segmentation of cerebrospinal fluid (CSF), white-matter (WM) and gray-matter (GM) was performed on the brain-extracted T1w using fast (FSL 5.0.9, RRID:SCR_002823, Zhang, Brady, and Smith 2001). Volume-based spatial normalization to one standard space (MNI152NLin2009cAsym) was performed through nonlinear registration with antsRegistration (ANTs 2.3.3), using brain-extracted versions of both T1w reference and the T1w template
Normalization template	ICBM 152 Nonlinear Asymmetrical template version 2009c

Noise and artifact removal

Principal components are estimated after high-pass filtering the preprocessed BOLD time-series (using a discrete cosine filter with 128s cut-off) for the two CompCor variants: temporal (tCompCor) and anatomical (aCompCor). tCompCor components are then calculated from the top 2% variable voxels within the brain mask. For aCompCor, three probabilistic masks (CSF, WM and combined CSF+WM) are generated in anatomical space.

Volume censoring

In ROI analysis spikes in the data, exceeding 4 times the voxel's standard deviation were applied de-spiking and were interpolated using the mean of one TRs engulfing each side of the outlier data point.

Statistical modeling & inference

Model type and settings

Intersubject representational similarity analysis (IS-RSA), and general linear model (GLM)

Effect(s) tested

To relate the semantic content with neural representation and to determine whether this representation differs in PTSD-related narratives, we conducted an intersubject representational similarity analysis (IS-RSA)

Specify type of analysis: ☐ Whole brain ☐ ROI-based ☒ Both

Anatomical location(s)

we extracted signals from bilateral hippocampus and amygdalausing the Harvard-Oxford probabilistic atlas to conduct region-of-interest (ROI) analyses. The PCC was demarcated functionally using a group level contrast

Statistic type for inference
(See Eklund et al. 2016)

In whole brain contrast statistical inference was made based on whole-brain statistical maps corrected for multiple comparisons using cluster size threshold family-wise error rate of p(FWE) < 0.01 for the identification and extraction of regions of interest (ROIs).

Correction

family-wise error rate of p(FWE) < 0.01 for GLM group contrasts. We tested the significance of IS-RSA by subjecting p-values of Spearman's correlation coefficients amassed across ROIs and conditions (e.g., 3 ROIs X 3 script types) by using a false-discovery rate (FDR) at q = 0.05

Models & analysis

n/a	Involved in the study
☒	☐ Functional and/or effective connectivity
☒	☐ Graph analysis
☐	☒ Multivariate modeling or predictive analysis

Multivariate modeling and predictive analysis

To relate the semantic content with neural representation and to determine whether this representation differs in PTSD-related narratives, we conducted an intersubject representational similarity analysis (IS-RSA)

We tested the significance of IS-RSA by subjecting p-values of Spearman's correlation coefficients amassed across ROIs and conditions (e.g., 3 ROIs X 3 script types) by using a false-discovery rate (FDR) at q = 0.05 implemented in MATLAB R2018a as function 'fdr_bh'.
To compare correlation coefficients between narrative types (e.g., 'PTSD' vs. 'Sad') we used two methods depending on groups' dependency: In cases where one variable is shared (e.g., correlation between CAPS and neural similarity in 'PTSD' narratives compared with correlation between the same CAPS data and neural similarity in 'Sad' narratives) we used Steiger test as implanted in 'r_test_paired.m' in MATLAB. Briefly, each correlation coefficient is converted into a z-score using Fisher's r-to-z transformation. Next the asymptotic covariance of the estimates is computed and are then used in an asymptotic z-test. We reported p-values from a two-tailed probability distribution. In contrast, in cases where the two comparisons had no shared components (e.g., correlation between semantic and neural similarity in 'PTSD' narratives and correlation between semantic and neural similarity in 'Sad' narratives), we used the 'corr_rtest' function in MATLAB to convert both correlation coefficient into z-score using Fisher's r-to-z transformation and calculate their absolute difference. This value was assigned a p value from a cumulative normal distribution function ('normcdf' in MATLAB). We report p-values from a two-tailed probability distribution.